LUND UNIVERSITY

Optical Diagnostics for Quantitative Potassium Chemistry in Biomass Thermochemical Conversion Processes

Weng, Wubin

2020

Document Version:
Publisher's PDF, also known as Version of record

Link to publication

Total number of authors:
1

Optical Diagnostics for Quantitative Potassium Chemistry in Biomass Thermochemical Conversion Processes

WUBIN WENG
DEPARTMENT OF PHYSICS | FACULTY OF ENGINEERING | LUND UNIVERSITY
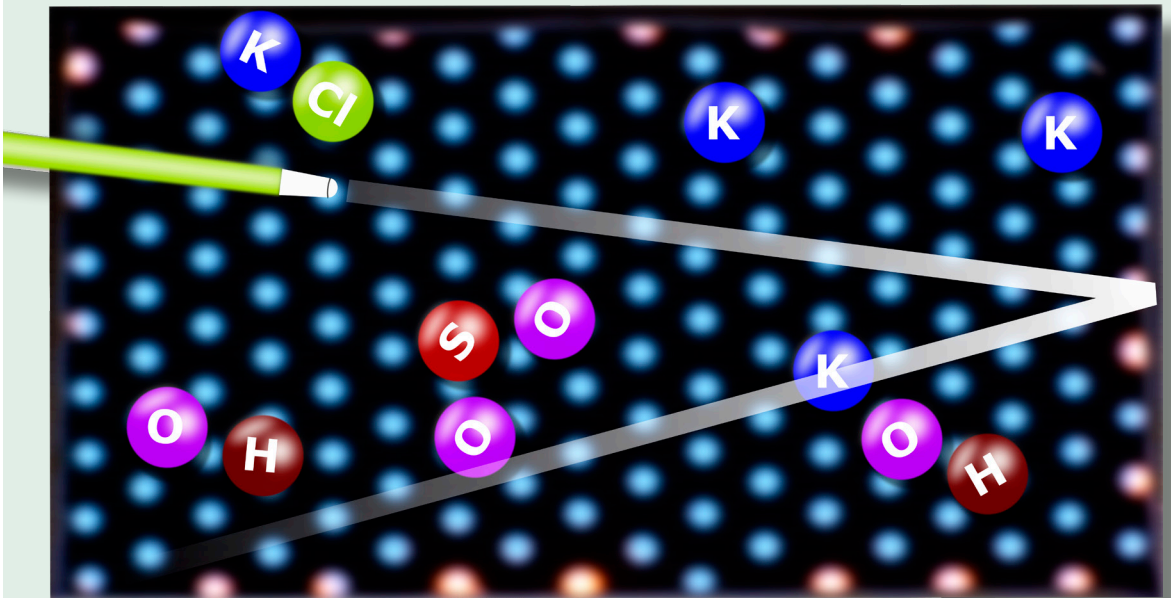
Optical Diagnostics for Quantitative Potassium Chemistry in Biomass Thermochemical Conversion Processes

Doctoral Dissertation

Wubin Weng

LUND
UNIVERSITY

DOCTORAL DISSERTATION

by due permission of the Faculty of Engineering, Lund University, Sweden.
To be defended in Rydbergsalen, Fysicum, Professorgatan I. 09:15 January 31, 2020.

Faculty opponent
Prof. Mikko Hupa
Chemical Engineering Department, Åbo Akademi University,
Turku, Finland

Organization LUND UNIVERSITY	Document name DOCTORAL DISSERTATION
Division of Combustion Physics Department of Physics PO Box 118, SE-221 00 LUND, Sweden	Date of issue January 31, 2020
	CODEN: LUTFD2/TFCP-220-SE
Author: Wubin Weng	Sponsoring organization

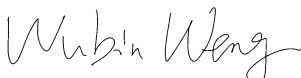Title and subtitle
Optical diagnostics for quantitative potassium chemistry in biomass thermochemical conversion processes

Abstract
Biomass is an essential sustainable and carbon-neutral energy source. Through thermochemical conversion processes, such as combustion and gasification, biomass can generally be used in boilers to provide heat and/or power. Biomass fuels contain varying amounts of potassium, chlorine and sulfur. The release of these elements, especially in the form of potassium chloride (KCl), in the thermal conversion processes causes crucial problems such as slagging and corrosion of heat transfer surface, and bed material agglomeration in operating furnaces. Potassium sulfate (K_2SO_4) is less corrosive and has a higher melting point than KCl. K_2SO_4 could be formed through sulfation of potassium using sulfur-containing additives, such as sulfur oxides (SO_2). Between KCl/KOH and SO_2, the sulfation can occur through gas-phase reactions. The understanding of the sulfation processes is based on gas-phase K-Cl-S chemistry, and the work in this thesis focuses on the development and application of in-situ optical diagnostics for quantitative measurements of key species in the K-Cl-S chemistry.

As a preliminary investigation (Paper I) of the homogeneous sulfation between gas-phase KCl/KOH and SO_2, a specially designed counter-flow reactor was adopted, where neither wall-based reactions nor other heterogeneous reactions could be involved. Homogenous sulfation was observed in the reactor, and the sulfation of KOH was observed to be more rapid than that of KCl. However, due to the counter-flow structure, quantitative measurement of potassium species was hard to be achieved. In order to achieve quantitative measurement and evaluate a detailed K-Cl-S mechanism, a laminar flame burner (Paper II) was designed to provide well-defined homogenous hot gas environments. The homogenous hot gas could be widely adjusted both in temperature and gas composition to mimic real operation conditions of furnaces. The temperature was measured using two-line atomic fluorescence (TLAF) thermometry. Different homogenous reactions could be investigated with seeding certain additives in gas or liquid phase, such as K_2CO_3, KCl and SO_2.

UV absorption spectroscopy was used to quantify concentrations of KOH, KCl, OH radicals and SO_2. However, UV absorption cross sections of KOH, KCl and SO_2 at the temperature over 1200 K were absent. Thus, they were accurately measured in this work (Paper III, IV). Tunable diode laser absorption spectroscopy (TDLAS) was adopted for the measurement of the concentration of K atoms. Two TDLAS systems, at 769.9 nm and 404.4 nm, were employed to extend the measurement dynamic range of potassium atoms, from below ppb-level to over ten ppm.

The K-Cl-S chemistry (Paper V, VI) was investigated in oxidative and reducing environments having temperatures from 1120 K to 1950 K with additives of K_2CO_3, KCl and SO_2. Based on the quantitative measurements of KOH, KCl, K atoms and OH radicals, a detailed K-Cl-S mechanism was evaluated and a reasonable agreement between the modelling and experimental results was obtained. SO_2 sulfated KOH/KCl to K_2SO_4 in an oxidative environment at a temperature below 1550 K. The sulfation of KOH was more rapid compared to that of KCl. The chain-terminating reactions between KOH / K atoms and OH radicals promoted the consumption of OH radicals and inhibited the oxidation of CO and H_2 as the environment temperature below 1550 K (Paper VII). Sulfation reactions consumed KOH and K atoms and eliminated the chain terminating reactions. In a reducing environment with SO_2 seeding, potassium was only transformed into KOSO, and UV absorption spectrum of KOSO was obtained for the first time.

Key words:
Optical diagnostics, Quantitative measurement, UV absorption spectroscopy, TDLAS, TLAF, Potassium chemistry, Sulfation, Biomass

Classification system and/or index terms (if any)

Supplementary bibliographical information		Language: English
ISSN and key title: 1102-8718		ISBN: 978-91-7895-372-1 (print) 978-91-7895-373-8 (pdf)
Recipient´s notes	Number of pages: 156	Price:
	Security classification	

I, the undersigned, being the copyright owner of the abstract of the above-mentioned dissertation, hereby grant to all reference sources permission to publish and disseminate the abstract of the above-mentioned dissertation.

Signature _Wubin Weng_   Date: December 12, 2019

Optical Diagnostics for Quantitative Potassium Chemistry in Biomass Thermochemical Conversion Processes

Doctoral Dissertation

Wubin Weng

LUND

UNIVERSITY

Division of Combustion Physics

Department of Physics

Contents

Abstract

Biomass is an essential sustainable and carbon-neutral energy source. Through thermochemical conversion processes, such as combustion and gasification, biomass can generally be used in boilers to provide heat and/or power. Biomass fuels contain varying amounts of potassium, chlorine and sulfur. The release of these elements, especially in the form of potassium chloride (KCl), in the thermal conversion processes causes crucial problems such as slagging and corrosion of heat transfer surface, and bed material agglomeration in operating furnaces. Potassium sulfate (K_2SO_4) is less corrosive and has a higher melting point than KCl. K_2SO_4 could be formed through sulfation of potassium using sulfur-containing additives, such as sulfur oxides (SO_2). Between KCl/KOH and SO_2, the sulfation can occur through gas-phase reactions. The understanding of the sulfation processes is based on gas-phase K-Cl-S chemistry, and the work in this thesis focuses on the development and application of in-situ optical diagnostics for quantitative measurements of key species in the K-Cl-S chemistry.

As a preliminary investigation (Paper I) of the homogeneous sulfation between gas-phase KCl/KOH and SO_2, a specially designed counter-flow reactor was adopted, where neither wall-based reactions nor other heterogeneous reactions could be involved. Homogenous sulfation was observed in the reactor, and the sulfation of KOH was observed to be more rapid than that of KCl. However, due to the counter-flow structure, quantitative measurement of potassium species was hard to be achieved. In order to achieve quantitative measurement and evaluate a detailed K-Cl-S mechanism, a laminar flame burner (Paper II) was designed to provide well-defined homogenous hot gas environments. The homogenous hot gas could be widely adjusted both in temperature and gas composition to mimic real operation conditions of furnaces. The temperature was measured using two-line atomic fluorescence (TLAF) thermometry. Different homogenous reactions could be investigated with seeding certain additives in gas or liquid phase, such as K_2CO_3, KCl and SO_2.

UV absorption spectroscopy was used to quantify concentrations of KOH, KCl, OH radicals and SO_2. However, UV absorption cross sections of KOH, KCl and SO_2 at the temperature over 1200 K were absent. Thus, they were accurately measured in this work (Paper III, IV). Tunable diode laser absorption spectroscopy (TDLAS) was adopted for the measurement of the concentration of K atoms. Two TDLAS systems, at 769.9 nm and 404.4 nm, were employed to extend the measurement dynamic range of potassium atoms, from below ppb-level to over ten ppm.

The K-Cl-S chemistry (Paper V, VI) was investigated in oxidative and reducing environments having temperatures from 1120 K to 1950 K with additives of K_2CO_3,

KCl and SO$_2$. Based on the quantitative measurements of KOH, KCl, K atoms and OH radicals, a detailed K-Cl-S mechanism was evaluated and a reasonable agreement between the modelling and experimental results was obtained. SO$_2$ sulfated KOH/KCl to K$_2$SO$_4$ in an oxidative environment at a temperature below 1550 K. The sulfation of KOH was more rapid compared to that of KCl. The chain-terminating reactions between KOH / K atoms and OH radicals promoted the consumption of OH radicals and inhibited the oxidation of CO and H$_2$ as the environment temperature below 1550 K (Paper VII). Sulfation reactions consumed KOH and K atoms and eliminated the chain terminating reactions. In a reducing environment with SO$_2$ seeding, potassium was only transformed into KOSO, and UV absorption spectrum of KOSO was obtained for the first time.

Popular science abstract

Global warming is one of the biggest worldwide challenges. Greenhouse gases emission during fossil-fuel utilization gives a dominant contribution. Therefore, increasing the share of renewable and carbon-neutral section in the total global energy consumption is nowadays a common sense. Common renewable energy resources can be biomass energy, hydropower, wind power, solar energy and geothermal energy.

Biomass energy is mainly from the organisms of plants. Forest wood and agriculture residues are the largest biomass energy sources. Different thermal conversion processes, such as pyrolysis, gasification and combustion, are regarded as the most important ways to use the biomass energy to generate power and heat directly, or produce syngas and bio-fuels including bioethanol and biodiesel. However, biomass usually contains relatively high concentrations of potassium, chlorine and sulfur, which may strongly influence the operation of boilers, pollutant emission and gas product quality. For example, potassium chloride causes problems of slagging and corrosion of heat transfer surface of boilers and bed material agglomeration. Potassium sulfate aerosols can be one of harmful emissions. Potassium species participate and affect various key reactions in the thermochemical processes of biomass fuels, and are found to be related to char and tar conversion.

In the present work, homogenous gas-phase potassium chemistry was investigated. The fundamental knowledge can support the utilization of biomass fuels with higher efficiency and lower emission. This thesis was mainly comprised of three parts: creating reaction environments, development and application of optical techniques for species measurements, and analysing the potassium chemistry through experimental and modelling approaches.

A burner with methane/air flames was designed to provide uniform hot flue gases, which were used as reaction environments. The temperature of the environments can be adjusted between 1000 K and 2000 K. Different reactants could be introduced into the hot flue gas homogenously, and their reactions were investigated in the present work. The concentrations of key species, such as KOH, KCl, K atoms, SO_2, and OH radicals, were quantified through non-intrusive and in-situ measurements using different absorption spectroscopy methods. In the absorption spectroscopy measurements, when collimated light passed through the hot flue gases, part of the light was absorbed by certain types of molecules or atoms. The molecules or atoms have their own characteristics in light absorption. KOH, KCl and SO_2 has broadband absorption at wavelength from 200 nm to 400 nm. OH radicals absorb the light at wavelength around 310 nm. K atoms have absorption exactly at 404.4 nm and 769.9 nm. Hence,

these species can be readily distinguished. Based on the amount of light that was absorbed, the concentration of the species in the hot flue gas could be calculated. The results show that the temperature and the oxygen concentration of the hot gas atmosphere strongly influenced the balance among different potassium species, mainly KOH, KCl, and K atoms. At a temperature lower than 1260 K, KOH could be readily sulfated by SO_2 and nucleation of K_2SO_4 occurred. KOH and K atoms in the hot flue gas enhanced the consumption of OH radicals, and consequently, inhibited the oxidation of CO and H_2 in the hot flue gas. In order to study the reactions pathways, a detailed K-Cl-S chemical mechanism was adopted to simulate the reactions under the experimental conditions.

List of papers

This thesis is based on following papers:

I.   **W. Weng,** S. Chen, H. Wu, P. Glarborg, Z. Li, *Optical Investigation of Gas-phase KCl/KOH Sulfation in Post Flame Conditions*, **Fuel** 224 (2018) 461-468.

II.   **W. Weng**, J. Borggren, B. Li, M. Aldén, Z. Li, *A Novel Multi-jet Burner for Hot Flue Gases of Wide Range of Temperatures and Compositions for Optical Diagnostics of Solid Fuels Gasification/Combustion*, **Review of Scientific Instruments** 88 (2017) 045104.

III.   **W. Weng,** C. Brackmann, T. Leffler, M. Aldén, Z. Li, *Ultraviolet Absorption Cross Sections of KOH and KCl for Nonintrusive Species-Specific Quantitative Detection in Hot Flue Gases,* **Analytical Chemistry** 91 (2019) 4719-4726.

IV.   **W. Weng,** M. Aldén, Z. Li, *Quantitative SO_2 Detection in Combustion Environments Using Broad Band Ultraviolet Absorption and Laser-Induced Fluorescence,* **Analytical Chemistry** 91 (2019) 10849-10855.

V.   **W. Weng,** Y. Zhang, H. Wu, P. Glarborg, Z. Li, *Optical Measurement of KOH, KCl and K for Quantitative K-Cl Chemistry in Thermochemical Conversion Processe*s, **Submitted.**

VI.   **W. Weng,** Z. Li, H. Wu, M. Aldén, P. Glarborg, *Quantitative K-Cl-S Chemistry in Thermochemical Conversion Processes Using In-situ Optical Diagnostics,* **Submitted.**

VII.   T.B. Vilches, **W. Weng,** M. Seemann, H. Thuman, Z. Li, P. Glarborg, *In Situ Quantitative Investigation of the Influence of Potassium on CO and H_2 Oxidation in Combustion Environments,* **To be submitted.**

VIII.   **W. Weng,** S. Li, M. Costa, Z. Li, *Quantitative Imaging of Potassium Release from Single Burning Pulverized Biomass Char Particles,* **Submitted.**

Related work

Papers not included in this thesis:

I.   **W. Weng,** T. Leffler, C. Brackmann, M. Aldén, Z. Li, *Spectrally Resolved Ultraviolet (UV) Absorption Cross-Sections of Alkali Hydroxides and Chlorides Measured in Hot Flue Gases,* **Applied Spectroscopy** 72 (2018) 1388-1395.

II.   **W. Weng,** M. Costa, Z. Li, M. Aldén, *Temporally and Spectrally Resolved Images of Single Burning Pulverized Wheat Straw Particles,* **Fuel** 224 (2018) 434-441.

III.   **W. Weng,** M. Costa, M. Aldén, Z. Li, *Single Particle Ignition and Combustion of Pulverized Pine Wood, Wheat Straw, Rice Husk and Grape Pomace,* **Proceedings of the Combustion Institute** 37 (2019) 2663-2671.

IV.   **W. Weng,** S. Li, M. Costa, Z. Li, *Burning Behavior and Potassium Release of Single Pulverized Biomass Char Particles*, **Submitted.**

V.   **W. Weng,** H. Feuk, S. Li, M. Richter, M. Aldeń, Z. Li, *Temporal Temperature Measurement on Burning Biomass Pellets Using Phosphor Thermometry and Two-line Atomic Fluorescence,* **Submitted.**

VI.   H. Fatehi, **W. Weng,** M. Costa, Z. Li, M. Rabaçal, M. Aldén, X.-S. Bai, *Numerical Simulation of Ignition Mode and Ignition Delay Time of Pulverized Biomass Particles,* **Combustion and Flame** 206 (2019) 400-410.

VII.   T. Leffler, C. Brackmann, **W. Weng,** Q. Gao, M. Aldén, Z. Li, *Experimental Investigations of Potassium Chemistry in Premixed Flames,* **Fuel** 203 (2017) 802-810.

VIII.   J. Borggren, **W. Weng,** A. Hosseinnia, P.-E. Bengtsson, M. Aldén, Z. Li, *Diode Laser-based Thermometry Using Two-line Atomic Fluorescence of Indium and Gallium,* **Applied Physics B** 123 (2017) 278.

IX.   J. Borggren, **W. Weng,** M. Aldén, Z. Li, *Spatially Resolved Temperature Measurements Above a Burning Wood Pellet Using Diode Laser-Based Two-Line Atomic Fluorescence,* **Applied Spectroscopy** 72 (2017) 964-970.

X.   D. Hot, R.L. Pedersen, **W. Weng,** Y. Zhang, M. Aldén, Z. Li, *Spatially and Temporally Resolved IR-DFWM Measurement of HCN Released from Gasification of Biomass Pellets,* **Proceedings of the Combustion Institute** 37 (2019) 1337-1344.

XI.   Q. Gao, **W. Weng,** B. Li, M. Aldén, Z. Li, *Gas Temperature Measurement Using Differential Optical Absorption Spectroscopy (DOAS),* **Applied Spectroscopy** 72 (2018) 1014-1020.

XII.   Q. Gao, **W. Weng,** B. Li, Z. Li, *Quantitative and Spatially Resolved Measurement of Atomic Potassium in Combustion Using Diode Laser,* **Chinese Physics Letters** 35 (2018) 024202.

XIII.   O. Hwang, M.C. Lee, **W. Weng,** Y. Zhang, Z. Li, *Development of Novel Ultrasonic Temperature Measurement Technology for Combustion Gas as a Potential Indicator of Combustion Instability Diagnostics,* **Applied Thermal Engineering** 159 (2019) 113905.

XIV.   K. Larsson, D. Hot, A. Ehn, A. Lantz, **W. Weng,** M. Aldén, J. Bood, *Quantitative Imaging of Ozone Vapor Using Photofragmentation Laser-Induced Fluorescence (LIF),* **Applied Spectroscopy** 71 (2017) 1578-1585.

Summary of papers

Paper I: Optical investigation of gas-phase KCl/KOH sulfation in post flame conditions.

W. Weng, S. Chen, H. Wu, P. Glarborg, Z. Li, Fuel 224 (2018) 461-468.

This paper investigated gas-phase sulfation and homogeneous nucleation of gas-phase KCl/KOH in a counter-flow reactor setup. SO_2 was used as sulfur source. Mie scattering was used to detect K_2SO_4 aerosols, and Rayleigh scattering was used to derive the temperature distribution. KOH was observed to be sulfated more readily than KCl. Oxidizing environment was needed to have the sulfation reactions. These characteristics were also predicted by modelling work.

I planned the experiment, and conducted the measurements together with S. Chen. I made all the data evaluation. I did the modelling work with the help from P. Glarborg. I wrote the manuscript with some input from the other authors.

Paper II: A novel multi-jet burner for hot flue gases of wide range of temperatures and compositions for optical diagnostics of solid fuels gasification/combustion.

W. Weng, J. Borggren, B. Li, M. Aldén, Z. Li, Review of Scientific Instruments 88 (2017) 045104.

A novel multi-jet burner was designed which can provide uniform hot flue gas with temperature ranging in 1000 K to 2000 K. Different additives in gas or liquid phase can be easily seeded into the hot flue gas for different homogeneous chemical reaction investigation. Solid fuels can be burned in the large uniform hot flue gas for the study of heterogeneous reactions. Different types of optical diagnostics can be easily applied in the burner.

I designed the burner and planned the experiment. The temperature measurements using TLAF and corresponding temperature calculation was conducted with the help of J. Borggren. I made most of the data evaluation. I wrote the manuscript with some input from the other authors.

Paper III: Ultraviolet absorption cross sections of KOH and KCl for nonintrusive species-specific quantitative detection in hot flue gases.

W. Weng, C. Brackmann, T. Leffler, M. Aldén, Z. Li, Analytical Chemistry 91 (2019) 4719-4726.

A method was newly developed to obtain the UV absorption cross-section of KOH and KCl in the combustion atmosphere having a temperature between 1300 K and 1800 K. The measurements of the cross-section relied on the accurate measurement of K atoms using TDLAS.

I planned the experiment, and conducted the measurements. I made all the data evaluation. I wrote the manuscript with some input from the other authors.

Paper IV: Quantitative SO_2 detection in combustion environments using broad band ultraviolet absorption and laser-induced fluorescence.

W. Weng, M. Aldén, Z. Li, Analytical Chemistry 91 (2019) 10849-10855.

SO_2 can be quantitatively detected in combustion environments based on the UV absorption cross-section of SO_2 obtained in the present work. The absorption cross-section strongly depended on the temperature. The laser-induced fluorescence of SO_2 at different temperature was also investigated for further achieving spatially resolved quantitative measurement of SO_2.

I planned the experiment, and conducted the measurements. I made the data evaluation. I wrote the manuscript with some input from the other authors.

Paper V: Optical measurement of KOH, KCl and K for quantitative K-Cl chemistry in thermochemical conversion processes.

W. Weng, Y. Zhang, H. Wu, P. Glarborg, Z. Li, Submitted.

The concentrations of KOH, KCl, and K atoms in the hot flue gas at temperatures ranging between 1120 K and 1950 K were quantitatively measured for the investigation of gas-phase K-Cl chemistry. Broadband UV absorption spectroscopy was applied for KOH/KCl measurements and TDLAS was applied for K atom measurements. Modelling work was conducted based on a detailed K-Cl mechanism. For most cases, the experimental and simulation results were in reasonable agreement.

I planned the experiment. The measurements were conducted with Y. Zhang. I made the data evaluation. I did the modelling work with the help from P. Glarborg. I wrote the manuscript with some input from the other authors.

Paper VI: Quantitative K-Cl-S chemistry in thermochemical conversion processes using in-situ optical diagnostics.

W. Weng, Z. Li, H. Wu, M. Aldén, P. Glarborg, Submitted.

The concentrations of KOH, KCl, K atoms, OH radicals and SO_2 in the hot flue gas at temperatures ranging between 1120 K and 1550 K were quantitatively measured for the investigation of gas-phase K-Cl-S chemistry. UV absorption spectroscopy was applied for KOH/KCl, SO_2 and OH radical measurements and TDLAS was applied for K atom measurements. K_2SO_4 aerosols were observed as illuminated by a green laser sheet. Modelling work was conducted based on a detailed K-Cl-S mechanism and predicted the experimental results.

I planned the experiment, and conducted the measurements. I made the data evaluation. I did the modelling work with the help from P. Glarborg. I wrote the manuscript with some input from the other authors.

Paper VII: In situ quantitative investigation of the influence of potassium on CO and H₂ oxidation in combustion environments.

T.B. Vilches, W. Weng, M. Seemann, H. Thuman, Z. Li, P. Glarborg, To be submitted.

The influence of potassium on the oxidation of CO and H_2 in the hot flue gas at the temperature between 1120 K and 1550 K and oxygen rich conditions was investigated. The concentrations of KOH and OH radicals were measured using UV absorption spectroscopy and the concentration of K atoms was measured using TDLAS. The concentrations of CO and H_2 were obtained using a GC system. A reduction of CO and H_2 oxidation was observed, which may be caused by the reduction of the concentration of OH radicals due to the existence of KOH and K atoms.

T.B. Vilches and me planned the experiment, conducted the measurements, and made the data evaluation. I was mainly responsible for the burner system, and the measurements of KOH, K atoms and OH radicals. T.B. Vilches was mainly

responsible for the measurement of CO and H_2. T.B. Vilches and me wrote the manuscript with some input from the other authors.

Paper VIII: Quantitative imaging of potassium release from single burning pulverized biomass char particles.

W. Weng, S. Li, M. Costa, Z. Li, Submitted.

Laser-induced photofragmentation fluorescence imaging technique was applied in the quantitative measurement of the potassium release from single burning pulverized wheat straw char particle with a size around 200 μm. The distribution of gas-phase KOH surrounding the burning char particle was obtained. About 0.034 μg potassium was released from the char particle with a residence time of 70 ms in the hot flue gas at 1650 K and having 6.5% oxygen.

I planned the experiment. The measurement was conducted with S. Li. The biomass char material was prepared and provided by M. Costa. I made the data evaluation. I wrote the manuscript with some input from the other authors.

Chapter **1**

Introduction

Nowadays, fossil fuels still have the biggest share in the global primary energy supply, and are considered to be the major contribution to global warming due to CO_2 emissions. The demands on renewable energy with net zero greenhouse gas emission are increasing. Biomass energy, together with other renewable energy sources, such as hydropower, wind power, solar energy and geothermal energy, will be a substantial section of the future energy supply. Thermal conversion processes, such as combustion, gasification, and pyrolysis, are considered the most important ways to use the biomass energy. Through thermal conversions, power and heat can be generated directly, and important carbon-based feedstock such as syngas and second generation biofuels can also be produced from biomass fuels.

Biomass, such as forest wood and agricultural residues, usually contains varying amounts of potassium, chlorine and sulfur [1, 2]. During thermal conversion, these elements can be released and may cause problems such as fouling, slagging, corrosion and bed material agglomeration in an operating furnace [3]. Suitable mitigation methods have been developed, such as the usage of sulfur-based additives [4-6] to convert KCl into K_2SO_4 which is less corrosive and has a higher melting point. Moreover, potassium, chlorine and sulfur potentially affect the overall thermal reaction process through producing or consuming radicals, such as OH, O and H, and may affect the pollutant formation [7] and product gas quality in gasification [8]. Thus, the understanding of potassium chemistry in homogeneous high-temperature environments is essential for a higher energy efficiency and lower pollutant emissions during the utilization of biomass fuels through different thermal conversion processes.

In previous works, detailed reaction mechanisms containing potassium, chlorine and sulfur reactions at high temperature have been reported [9-12]. However, model validation is difficult. Despite that some experimental studies about potassium chemistry have been conducted [11, 13-15], more experiments under well-defined conditions with accurate measurements from optical diagnostics are still required to further evaluate mechanisms.

In the present work, the research questions/focus are listed:

1. Does sulfation occur via homogenous reactions between gas-phase KCl/KOH and SO_2?
2. To provide uniform hot gas environments for homogenous gas-phase potassium reactions, a new burner needs to be developed.
3. How can the concentrations of KOH, KCl, K atoms, SO_2 and OH radicals be quantitatively measured using non-intrusive optical techniques?
4. Absorption spectroscopy was employed for concentration measurements. What will be the UV absorption cross-sections of KOH, KCl and SO_2 in a hot gas environment with a temperature over 1000 K?
5. How do the reaction environments influence the formation of potassium species and the potassium sulfation process?
6. Will potassium species affect the radical consumption and fuel oxidation?
7. Can simulations with the present detailed K-Cl-S mechanism predict our experiment results?

Thus, the thesis work is divided into the following parts: preliminary investigations, design of a new burner for providing reaction atmospheres, development and application of new optical methods for key species measurements, and experiments and simulations for deepened understanding of potassium chemistry.

Chapter 2 presents the work on the preliminary investigations of homogenous sulfation reactions between KCl/KOH and SO_2 in different hot gas environments. A counter-flow reactor was designed to avoid any wall-based reactions and heterogeneous reactions. K_2SO_4 aerosols formed in the sulfation were observed through the illumination by a laser sheet. Chapter 3 describes further investigations with quantitative measurements, where a novel laminar flame burner was designed to provide uniform hot gas environments for homogeneous K-Cl-S reactions. The temperature of the hot gas environment can be widely adjusted, between 1000 K and 2000 K. Different optical diagnostics can be readily applied on the burner. In the present work, mainly broadband UV absorption spectroscopy and tunable diode laser absorption spectroscopy was adopted for measurements of concentrations of KOH,

KCl, K atoms, SO$_2$, and OH radicals. For quantitative analysis, the UV absorption cross sections of KOH, KCl and SO$_2$ in combustion atmosphere were measured. In Chapter 4, K-Cl-S chemistry was studied in hot gas environments with different temperatures and oxygen concentrations. Corresponding simulation work was conducted with a detailed K-Cl-S mechanism. The discussion focused on the formation of different potassium species, the sulfation process and effects of potassium on OH consumption and CO/H$_2$ oxidation in different gas environments.

Chapter 2

# Investigation of potassium sulfation

There are several studies on the homogeneous sulfation process between gas-phase KOH/KCl and SO_2. A detailed mechanism including K-Cl-S chemistry has been developed by Glarborg and Hindiyarti et al. [9, 10]. However, experimental studies conducted on this topic are still scarce. Through experimental measurements Li et al. [11] have verified that the formation of K_2SO_4 could occur between gas-phase KCl and SO_2. As the first part of this thesis work, a new reactor was designed to investigate the sulfation of both KOH and KCl. The advantage of the reactor is that it can completely avoid any wall-based and heterogeneous reactions.

2.1 Experimental setup and simulation

As presented in Paper I, the preliminary investigation of the sulfation process was conducted in a counter-flow setup, as shown in Figure 2.1. The advantage of this setup is to allow only homogenous reactions between gas-phase KCl/KOH and SO_2 to occur while avoiding any wall-based or heterogeneous reactions, since the sulfation reactions could only occur in the mixing region, which was located away from the burner surfaces.

A Perkin-Elmer burner was used to generate uniform laminar flows of hot flue gases from premixed CH_4/air flames. The flat premixed flame with a diameter of 23 mm attached on the surface of the burner. The fuel-air equivalence ratio of the premixed flame was adjusted to be 0.9 or 1.1 to generate an oxidizing or reducing environment, respectively. A well-prepared KOH or KCl aqueous solution was atomized by a

nebulizer and transported by the premixed CH_4/air gas flow to the flame, which enabled a homogeneous introduction of KOH or KCl. When KOH or KCl passed the premixed flame front, which had a high temperature over 2000 K, gas-phase KOH and/or KCl was generated. The concentration of potassium in the hot flue gas was calculated to be around 215 ppm according to the consumption rate of the aqueous solution. A N_2 flow surrounding the premixed flame was used to shield the flame from the ambient air.
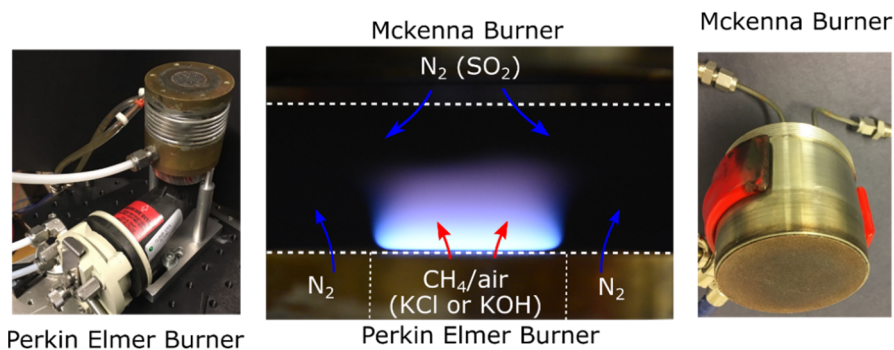
Figure 2.1
Photo of the counter-flow system with flames (middle), Perkin Elmer burner (left), and Mckenna burner (right).

A sintered-metal porous plug of a McKenna burner with a diameter of 60 mm was placed above the Perkin-Elmer burner to supply a N_2 flow containing a certain amount of SO_2, as shown in Figure 2.1. The hot flue gas flow from the Perkin-Elmer burner and the N_2/SO_2 flow from the McKenna burner encountered each other, thus a counter-flow structure was generated. The concentration of SO_2 in the N_2 flow was set to be 0 ppm, 245 ppm or 980 ppm.

Sulfation reactions between SO_2 and KCl/KOH occurred in the mixing region, where K_2SO_4 was formed. Since K_2SO_4 has a high boiling point, aerosols of K_2SO_4 were generated after nucleation. In order to detect the aerosols, a vertical laser sheet was sent through the counter-flow region to illuminate the aerosols. The laser beam was produced from the third harmonic of a Nd:YAG laser (Brilliant B, Quantel). It has a wavelength of 355 nm and a pulse energy of ~50 mJ. The Mie scattering signal from the aerosols was captured by an ICCD camera. Meanwhile, in the same system, the temperature distribution of the counter-flow was obtained based on Rayleigh scattering, as presented in Paper I.

A one-dimensional opposed-flow model in Chemkin-Pro [16] was used to simulate the sulfation process occurring in the counter-flow reactor. A potassium sulfation mechanism was adopted based on previous works [9-11]. The composition of the two

inlets of the model was set to be the composition of the hot flue gas of the premixed flame on Perkin-Elmer burner and the N_2 flow with a certain amount of SO_2 from the Mckenna burner, respectively. The composition of the hot flue gas was obtained through the calculation using a one-dimensional free propagation premixed flame model in Chemin-Pro with the GRI-3.0 mechanism [17]. In the calculation, the hot flue gas at 3 mm from the flame front was used, which had a temperature of 2060 K for the fuel-lean case and 2118 K for the fuel-rich case. The axial distance in the model was set to be 20 mm.

2.2 Preliminary results and discussion

The distribution of the Mie scattering signal from the aerosols in the hot flue gas produced in the fuel-lean case with KCl seeding is shown in Figure 2.2 (a). When the hot flue gas with gas-phase KCl was cooled by the surrounding N_2 co-flow or the N_2 from the top through the Mckenna burner, KCl aerosols were formed and Mie scattering was observed in the region having a temperature between 700 K and 1000 K according to the temperature measurement using Rayleigh scattering thermometry. When SO_2 was introduced into the counter-flow through the Mckenna burner, a much stronger Mie scattering was observed as shown in Figure 2.2 (b). The images in Figure 2.2 (a) and Figure 2.2 (b) were put together in Figure 2.2 (c), and it was found that compared to the case without SO_2 seeding, the location of the Mie scattering in the case with SO_2 seeding shifted a bit to the hot flow side, where the temperature was between 1000 K and 1400 K. This indicates that K_2SO_4 was generated and the nucleation occurred, since K_2SO_4 has a much lower vapour pressure and condenses at a higher temperature than KCl [18].
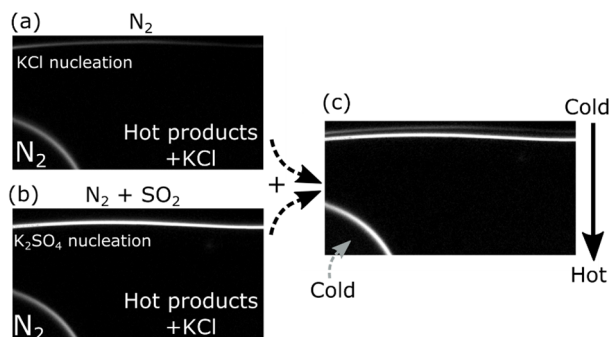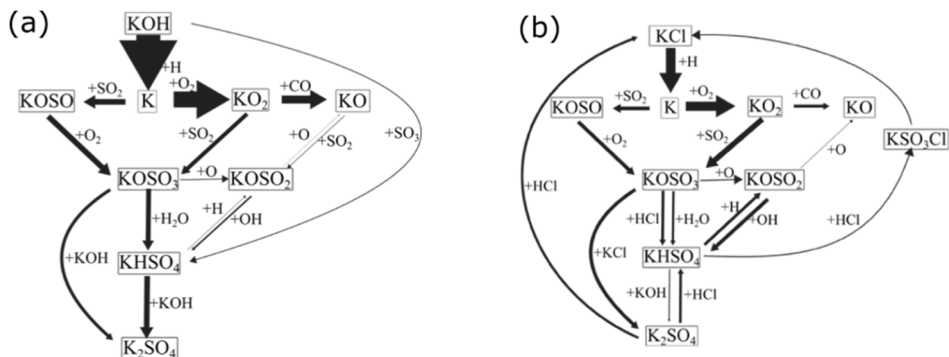

Figure 2.2
Images of the Mie scattering signals in the counter-flow by the KCl seeded fuel-lean hot flue gas and the N_2 flow illuminated with a thin laser sheet without (a) and with (b) SO_2, and combination (c) of these two images.
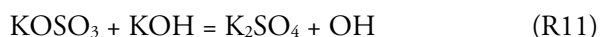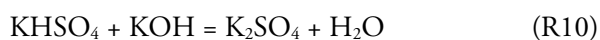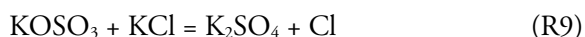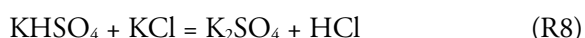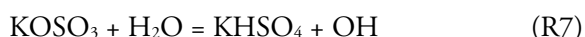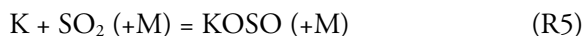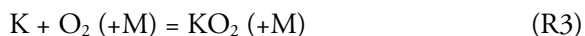
Similar to the case with KCl seeding, K_2SO_4 aerosols were also detected in the counter-flow with KOH and SO_2 seeding. The Mie scattering signal in the case with KOH seeding was much stronger than the one with KCl seeding, which indicates that the homogeneous sulfation of KOH occurred more readily than the one of KCl. When the flame was switched to the fuel-rich case, the Mie scattering signal became more than 10 times weaker than the one in the fuel-lean case, since oxidation is necessary in the sulfation reactions between gas-phase KOH/KCl and SO_2.

The simulation results including the distributions of temperature and the concentrations of potassium and sulfur species along the counter-flow vertical axis were presented in Paper I. The predicted temperature distribution showed good agreement with the experimental one. In the flow with KOH/KCl and SO_2 seeding, K_2SO_4 was generated in the region having a temperature around 1200 K. About five times more K_2SO_4 was predicted to be formed in the case with KOH than the case with KCl. Almost no K_2SO_4 was formed in the fuel-rich case.

Figure 2.3
Reaction pathways for the formation of K_2SO_4 at 1200 K in the counter-flow comprised by fuel-lean hot flue gas with KOH (a) or KCl (b) seeding and the N_2 flow containing SO_2

The pathways of sulfation between KOH/KCl and SO_2 in the fuel-lean case were analysed and the results are presented in Figure 2.3. The sulfation was predicted to occur mainly through the following reactions:

$$KOH + H = K + H_2O \qquad \text{(R1)}$$

$$KCl + H = K + HCl \qquad \text{(R2)}$$

$$K + O_2 (+M) = KO_2 (+M) \qquad \text{(R3)}$$

$$KO_2 + SO_2 (+M) = KOSO_3 (+M) \qquad \text{(R4)}$$

$$K + SO_2 (+M) = KOSO (+M) \qquad \text{(R5)}$$

$$KOSO + O_2 (+M) = KOSO_3 (+M) \qquad \text{(R6)}$$

$$KOSO_3 + H_2O = KHSO_4 + OH \qquad \text{(R7)}$$

$$KHSO_4 + KCl = K_2SO_4 + HCl \qquad \text{(R8)}$$

$$KOSO_3 + KCl = K_2SO_4 + Cl \qquad \text{(R9)}$$

$$KHSO_4 + KOH = K_2SO_4 + H_2O \qquad \text{(R10)}$$

$$KOSO_3 + KOH = K_2SO_4 + OH \qquad \text{(R11)}$$

First, K atoms are generated through reaction R1 and R2. Then, $KOSO_3$ is formed through the reactions between K atoms, O_2 and SO_2 (R3 – R6). Finally, $KOSO_3$ reacts with KCl, KOH or H_2O to generate K_2SO_4 or $KHSO_4$ (R7 – R11). It can be seen that the sulfation highly depends on the concentration of K atoms. Since the lower thermal stability of KOH facilitates the formation of more atomic K compared to KCl, the sulfation of KOH has a higher propensity than that of KCl. In the sulfation of potassium by SO_2, O_2 plays an important role in reaction R3 and R6 to generate $KOSO_3$. Hence in the fuel-rich case, K_2SO_4 cannot be formed and a large amount of KOSO is generated instead.

However, in order to evaluated the K-Cl-S mechanism directly for a better understanding of the sulfation process, quantitative measurements on the concentrations of KOH, KCl, K atoms, SO_2 and OH radials are needed. This therefore becomes the focus of the rest of the thesis.
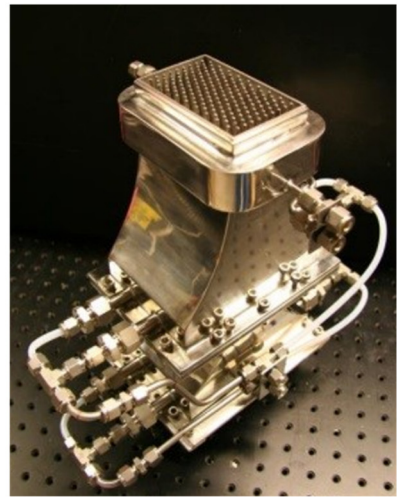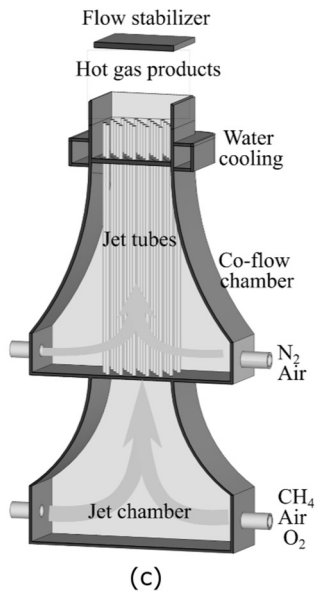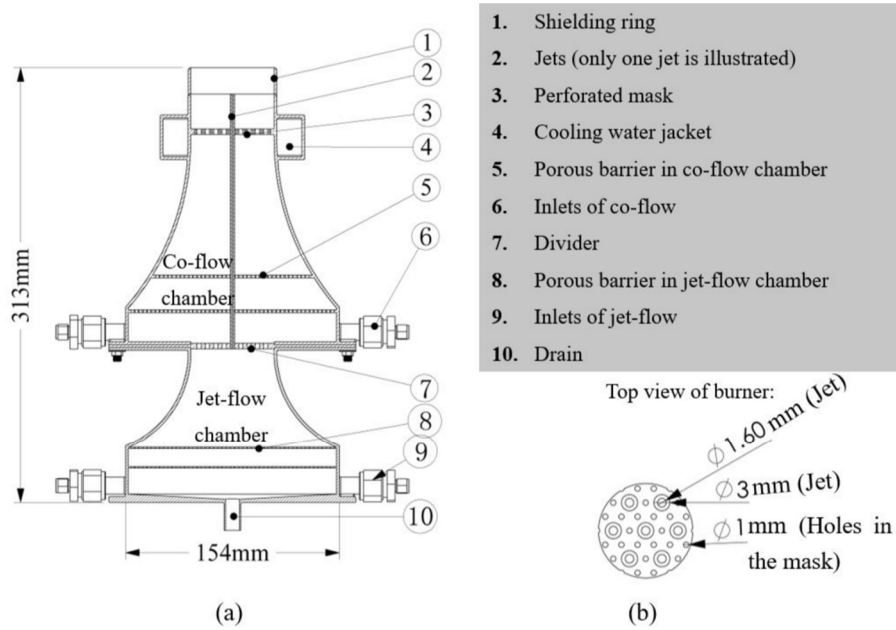
Chapter 3

Burner design and in situ quantitative measurements

Absorption spectroscopy provides feasible techniques for quantitative concentration measurements. However, limited by the line-of-sight nature of these techniques, it is a big challenge to measure the concentration of key species in the mixing zone of the counter-flow reactor due to the large concentration gradient. Thus, homogenous reaction environments are needed. In the present work, a new burner was designed which provided uniform hot gas environments. Because of the uniformity, absorption spectroscopic techniques can be easily applied. The gas environment has a wide range of temperature and composition to mimic different reaction atmospheres. Broadband UV absorption spectroscopy was employed for measurements of concentrations of KOH, KCl, SO_2 and OH radicals. Tunable diode laser absorption spectroscopy was used for concentration measurements of K atoms.

3.1 Multi-jet burner

The newly designed burner is shown in Figure 3.1 with its photo, 3D structure and sectional view. It is mainly comprised of two chambers, jet-flow chamber and co-flow chamber, separated by a divider (7). The jet flows, mainly CH_4/air/O_2, are introduced into the jet-flow chamber through four inlets (9). With two porous barriers (8) and the parabolic convergent shape of the chamber, the jet-flow can be evenly distributed into

1. Shielding ring
2. Jets (only one jet is illustrated)
3. Perforated mask
4. Cooling water jacket
5. Porous barrier in co-flow chamber
6. Inlets of co-flow
7. Divider
8. Porous barrier in jet-flow chamber
9. Inlets of jet-flow
10. Drain

Top view of burner:

$\phi 1.60$ mm (Jet)

$\phi 3$ mm (Jet)

$\phi 1$ mm (Holes in the mask)

Co-flow chamber

Jet-flow chamber

313mm

154mm

(a)

(b)

Flow stabilizer

Hot gas products

Water cooling

Jet tubes

Co-flow chamber

N_2
Air

Jet chamber

CH_4
Air
O_2

(c)

(d)

Figure 3.1
The structure of the burner. (a) Sectional view of the burner. (b) Partial top view of the burner. (c) 3D structure of the burner. (d) Photo of the burner.

181 jet tubes (2). These jet tubes have inner and outer diameter of 1.6 mm and 3 mm, respectively. Above each jet tube, a laminar premixed conical flame is stabilized, producing hot gas products. A photo with the typical jet flame matrix is presented in Figure 3.2 (a). Meanwhile, a co-flow is introduced into the co-flow chamber, and a uniform laminar flow is obtained as the flow passes through the two porous barriers (5). After a perforated mask (3) and several layers of 1 mm diameter glass beads, the co-flow can be evenly mixed with the hot products from the jet tubes. After the shielding ring (1), above the burner outlet, a homogenous hot gas environment is generated. The temperature and the composition of the hot gas products can be readily adjusted by varying the gas composition of the jet-flow and the co-flow. This is different from other flat flame burners, such as the McKenna burner [19], Meker burner [20], and Perkin-Elmer burner [21], which can only use a limited number of flat-flame cases to provide hot gas environment. The rectangular burner outlet had a size of ~85 mm × 47 mm, and the large size is in favour for the application of absorption spectroscopy techniques.
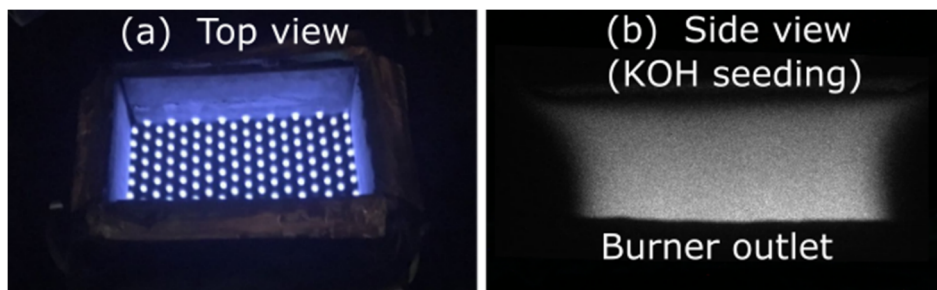
Figure 3.2
Photo of the burner head with flames on (a) and chemiluminescence of K atom at 766 nm in hot flue gas with KOH seeding capture by ICCD camera (b).
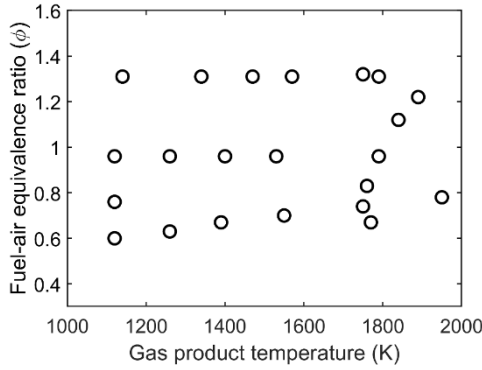
The flame conditions adopted in the present work are summarized in Table 3.1 with variation in temperature of gas product and fuel-air equivalence ratio. The temperature at ~5 mm above the burner outlet was measured using two-line atomic fluorescence thermometry with indium atoms as reported by Borggren et al. [22], and the details of the measurements will be described in the next section. The accuracy of the measurements was evaluated to be ~2.7% [22]. The temperature varies in the range between 1120 K and 1950 K. The equivalence ratio was varied between 0.6 and 1.31 to obtain hot gas products with different oxygen concentrations. The fuel-air equivalence ratio was calculated based on the total fuel and oxygen from both jet-flow and co-flow. The fuel-lean cases with equivalence ratio smaller than 1.0 will result in certain amounts of oxygen in the hot flue gas, while for the fuel-rich case with equivalence ratio over 1.0, the hot flue gas will be oxygen free. For example, the cases

with equivalence ratio of 0.6 and 0.96 have O_2 concentration of about 4.5% and 0.5%, respectively. The distribution of the temperature and equivalence ratio of all the flame cases are summarized in Figure 3.3.

Table 3.1
Summary of the flame conditions adopted in this experiment, where the temperature measurement was performed at a location 5 mm above the burner outlet.

| Flame Case | Gas flow rate (sl/min) | | | | | Fuel-air equivalence ratio φ | Gas product temperature (K) |
| | Jet-flow | | | Co-flow | | | |
	CH_4	Air	O_2	N_2	Air		
T2O1	2.66	17.34	1.89	6.96	11.61	0.67	1770
T2O2	2.66	17.34	1.89	10.83	7.74	0.74	1750
T2O3	2.66	17.34	1.89	14.21	4.38	0.83	1760
T2O4	2.66	17.34	1.89	18.60	0.00	0.96	1790
T2O5	3.04	17.11	1.86	13.95	0.00	1.12	1840
T2O6	3.14	15.53	1.91	12.09	0.00	1.22	1890
T2O7	3.23	14.16	1.93	9.30	0.00	1.32	1750
T1O2	2.95	19.20	2.09	6.84	7.09	0.78	1950
T3O2	2.47	12.23	2.58	18.97	8.90	0.70	1550
T3O4	2.47	12.23	2.58	27.90	0.00	0.96	1530
T4O2	2.28	11.89	2.26	22.69	9.83	0.67	1390
T4O4	2.28	11.89	2.26	32.55	0.00	0.96	1400
T5O2	2.09	10.90	2.07	26.50	10.66	0.63	1260
T5O4	2.09	10.90	2.07	37.20	0.00	0.96	1260
T6O2	1.71	8.91	1.69	26.92	10.25	0.60	1120
T6O3	1.71	8.91	1.69	32.55	4.65	0.76	1120
T6O4	1.71	8.91	1.69	37.20	0.00	0.96	1120
T1O7	3.62	13.76	2.61	11.16	0.00	1.31	1790
T3O7	3.04	10.14	2.51	13.95	0.00	1.31	1570
T4O7	2.66	9.12	2.14	18.60	0.00	1.31	1470
T5O7	2.47	8.47	1.99	22.32	0.00	1.31	1340
T6O7	2.28	7.82	1.84	27.90	0.00	1.31	1140

Figure 3.3
Distribution of gas product temperature and fuel-air equivalence ratio of the flame conditions used in the present work.
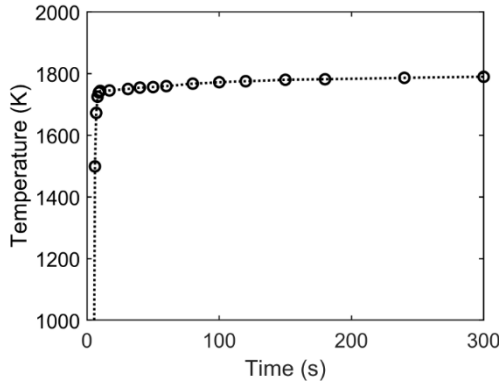
Figure 3.4
Variation of the hot flue gas temperature after the start-up of the burner.

Compared to high-temperature reactors/furnaces operated with electric heating, the biggest advantage of a burner is its short start-up time. Especially in the present burner, the hot flue gases with temperatures over 1550 K are produced by lifted flames. This design highly reduces the heat loss to the burner. Figure 3.4 presents the temperature variation of the hot gas products as a function of the time after the start-up of the burner. It can be seen that the temperature can stabilize at a certain value in a short time, typically less than 1 min.

Potassium and chlorine was introduced into the hot gas environments through the jet-flows. Potassium carbonate or potassium chloride was prepared in water solutions with a concentration of 0.5 mol/l and 1.0 mol/l, respectively. The solution was atomized with an ultrasonic fog generator. The resulting fog was transported into the jet-flow

33

chamber and mixed into premixed jet flow. When the fog droplets passed through the premixed flame fronts with a temperature over 2000 K, KCl was vaporized into gas-phase KCl directly and K_2CO_3 can react rapidly with water vapour to form gas-phase KOH. In the following work, K_2CO_3 water solution was adopted instead of KOH solution that was used in our preliminary investigations in the Perkin-Elmer burner in Chapter 2, since K_2CO_3 solution is much less corrosive than KOH solution. In Figure 3.2 (b), the image shows the signal of the chemiluminescence of K atoms in the hot flue gas with KOH seeding captured by an ICCD camera with an interference band pass filter centred at 766 nm. It can be seen that uniform signal was obtained along the horizontal direction, which indicates that the seeded additives can be homogeneously distributed in the hot flue gas environments.

3.2 Temperature measurements

The temperature of the hot gas products 5 mm over the burner outlet was measured using two-line atomic fluorescence (TLAF) thermometry with indium atoms. The detail of the measurement has been reported by Borggren et al. [22]. In TLAF, the indium atoms at two different lower energy levels, cf. level 1 and level 2 in Figure 3.5 (a), are excited by the lasers at 410 nm and 451 nm to a common higher energy level, cf. level 3 in Figure 3.5 (a). When the excited atoms relax back to the two low energy levels, fluorescence is generated, cf. F_{31} and F_{32} in Figure 3.5 (a). The strength of the fluorescence generated from the two different excitations is proportional to the population of the two lower levels, which is governed by the temperature-dependent Boltzmann distribution, and the correlation between the fluorescence ratio and temperature is presented by the curve in Figure 3.5 (b).
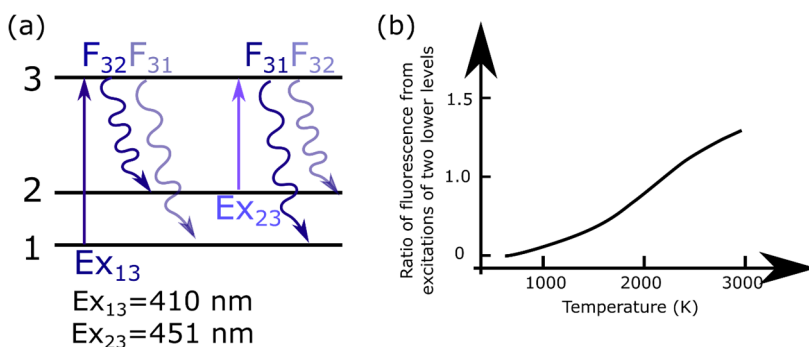
Figure 3.5
Simplified energy level diagram of the indium atom (a) and the correlation between the ratio of fluorescence and temperature (b).

In the present work, the fluorescence ratio obtained in experiments was compared to the one obtained in simulations. In the experiment, the fluorescence was recorded by a camera, and the ratio of the fluorescence after compensation for laser power is given by [22],

$$R_{exp} = \frac{F_2/I_{23}}{F_1/I_{13}} \qquad (3.1)$$

where F_1 and F_2 are the fluorescence signals generated from the excitation of energy level 1 and level 2, respectively, and I_{13} and I_{23} is the power of the laser at 410 nm and 451 nm, respectively. In the simulations, the fluorescence ratio is expressed as [22],

$$R_{sim}(T) = \frac{g_{23}(\lambda_{23},T) \cdot f_2(T) \cdot B_{23}}{g_{13}(\lambda_{13},T) \cdot f_1(T) \cdot B_{13}} \qquad (3.2)$$

where g is the line shape as a function of wavelength (λ) and temperature (T), f is the Boltzmann distribution and B is the Einstein absorption coefficient. Combining Equation 3.1 and Equation 3.2, the temperature is derived.

The temperature measurement system adopted is similar to the one developed by Borggren et al. [22], as shown in Figure 3.6. Two external cavity diode lasers (Toptica, DL 100pro and DL 100) generated two continuous-wave beams at 410 nm and 451 nm. These two lasers were used to probe the indium transitions $5^2P_{1/2} \rightarrow 6^2S_{1/2}$ (Ex$_{13}$ in Figure 3.5 (a)) and $5^2P_{3/2} \rightarrow 6^2S_{1/2}$ (Ex$_{23}$ in Figure 3.5 (a)), respectively, with a power around 5 mW. The lasers were overlapped using a dichroic mirror, and passed through the measurement zone alternately using a chopper. The wavelength and the power was monitored by a wavemeter and photodiodes, respectively.

When the laser passed through the hot flue gas, the indium atoms there were excited and emitted fluorescence. The fluorescence was captured by an ICCD camera through an interference band pass filter with a centre wavelength of 450 nm and full width at half maximum (FWHM) of ±5 nm. A typical photo of the fluorescence above the burner captured by a digital camera is shown in Figure 3.6. Trimethylindium (TMI) or indium chloride (InCl$_3$) was introduced into the gas products to generate indium atoms. For TMI seeding, a system developed by Whiddon et al. [23] was used. InCl$_3$ was seeded into the hot flue gas through an atomized InCl$_3$ water solution using an ultrasonic fog generator, as described above for potassium seeding.
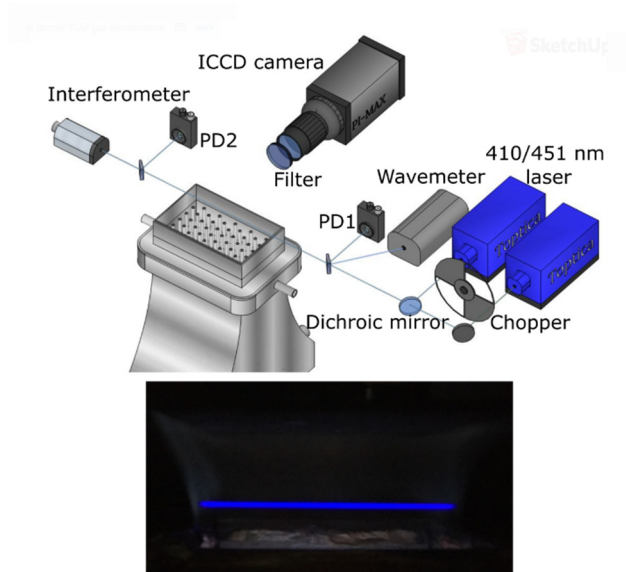
Figure 3.6
Schematic setup for the TLAF system and a photo of the burner outlet with laser-induced fluorescence of indium atoms.
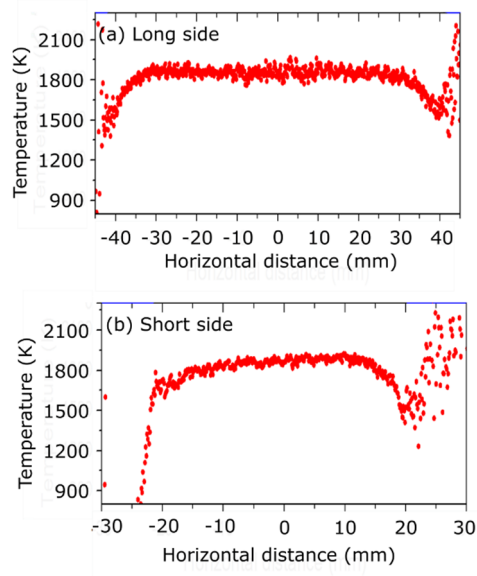
Figure 3.7
Horizontal distribution of the hot gas product temperature along the long side (a) and the short side (b) of the burner outlet measured with TLAF.

As presented in Paper II, through the fluorescence distribution obtained from an ICCD camera, the one-dimensional horizontal temperature distribution was derived. The typical horizontal distributions of the temperature along the long side and short side of the burner are shown in Figure 3.7. The homogenous hot flue gas area is estimated to be larger than 70 mm × 40 mm. It should be noted that at the edge of the hot flue gas, the measured temperature became less reliable due to the low indium atom concentration that resulted in weak fluorescence signal.

3.3 K atoms measurement

Tunable diode laser absorption spectroscopy (TDLAS), based on the Beer-Lambert law, is adopted for the quantitative concentration measurements of potassium atoms. Two transitions employed in the present work to probe the potassium atoms are shown in Figure 3.8. According to the Beer-Lambert law [24, 25], the frequency-dependent absorbance, $\alpha(\nu)$, is given by,

$$\alpha(\nu) = -\ln(\frac{I(\nu)}{I_0(\nu)}) = \sigma(\nu) \cdot L \cdot N \tag{3.3}$$

where ν is the frequency of the light, I_0 and I is the intensity of the light before and after passing through the flue gas with potassium atoms, respectively, σ is the absorption cross section as a function of frequency, L is optical path length and N is the number density of potassium atoms. The absorption cross section can be expressed as,

$$\sigma(\nu) = \frac{h\nu_0 B_{12} g(\nu,N,T)}{c} \tag{3.4}$$

where h is Plank constant, ν_0 is the transition central frequency, B_{12} is the Einstein absorption coefficient from ground state to excited state, g is the area-normalized line shape and c is the speed of light. Thus, the number density can be obtained by integrating over Equation 3.4, and expressed as,

$$N = \frac{c}{h\nu_0 B_{12} L} \int \alpha(\nu) \, d\nu \tag{3.5}$$
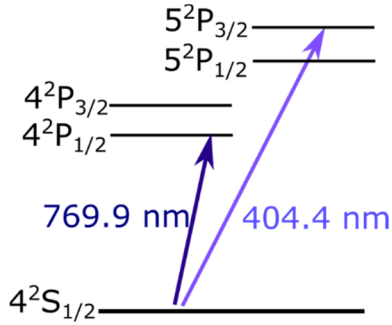
Figure 3.8
Partial energy level diagram of the potassium atom including the resonant transitions at 769.9 nm and 404.4 nm.
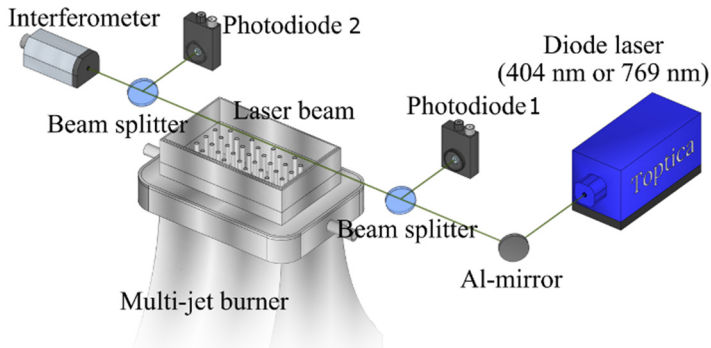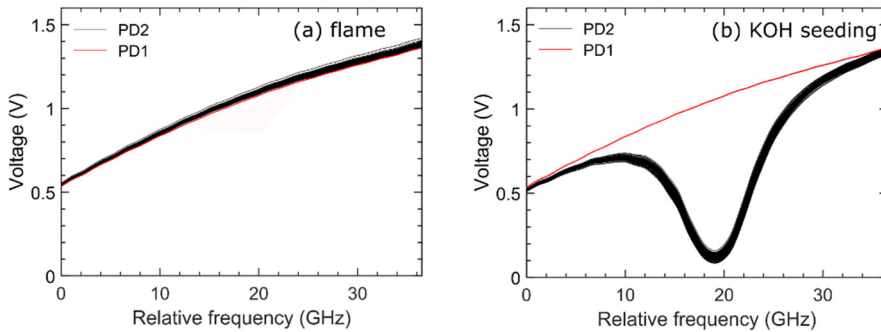

Figure 3.9
Schematic setup for the TDLAS system for K-atom measurement.

In previous works [24-26] for measurements of potassium atoms, a TDLAS system at 769.9 nm was widely used with a high measurement sensitivity. The schematic of the experimental setup employed in present thesis work with 769.9 nm laser is shown in Figure 3.9. An external cavity laser (Toptica) was used to produce laser light with a wavelength at 769.9 nm probing the potassium $4^2S_{1/2} \rightarrow 4^2P_{1/2}$ transition. The wavelength was scanned a certain range at a repetition rate of 100 Hz using a scan control module. The scanning range was monitored by a high-finesse confocal Fabry-Perot etalon and the power of the laser before and after the passage of the hot flue gas was measured by two photodiodes.
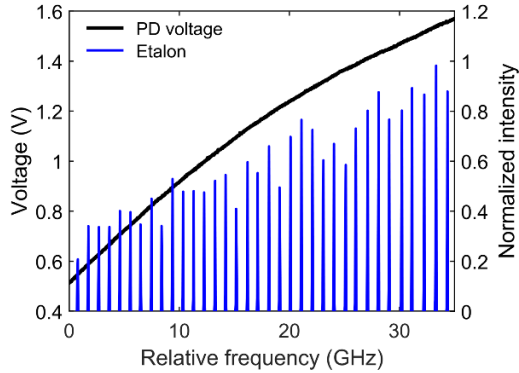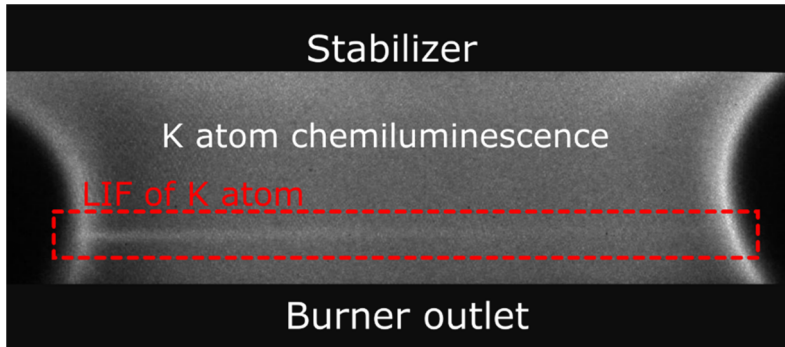
Figure 3.10
Voltage of the photodiode detecting the light without passing the hot flue gas, and the signal of etalon with a free spectral range of 1 GHz.
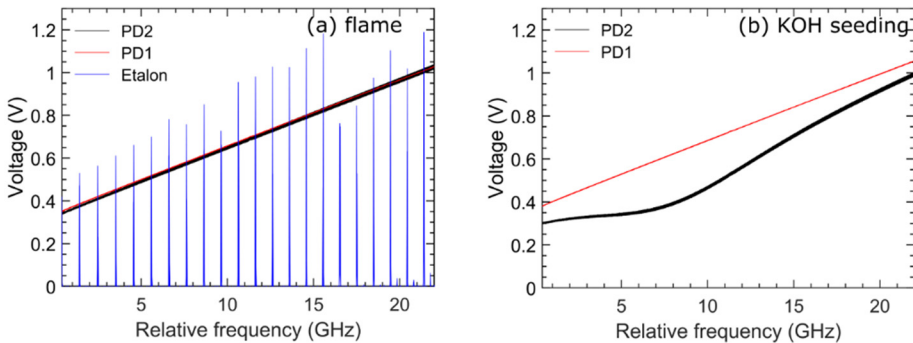

Figure 3.11
Voltage of the photodiodes detecting the light before and after passing through the hot flue gas as a function of laser frequency without (a) and with (b) KOH seeding in the 769.9 nm TDLAS system. The potassium concentration in (b) was calculated to be 0.05 ppm.

As shown in Figure 3.10, the 769.9 nm laser had a scanning range over 35 GHz, and the voltage of the photodiode, representing the power of the laser, varied smoothly with the light frequency. The voltage of the photodiodes detecting the laser after the passage of the hot flue gas with or without KOH seeding is presented in Figure 3.11, which was based on 50 measurements. In Figure 3.11 (b), a significant absorption can be observed with about 20 ppm KOH seeding. Based on the absorption, the concentration of K atoms in the hot flue gas was calculated to be 0.05 ppm through the data process described in detail in Paper III. Moreover, it can be noted that the signal from the photodiode detecting the laser after the passage of the hot flue gas was more scattered than the one before the passage of the hot flue gas. It was mainly caused by fluctuations of the hot flames.

39

Figure 3.12
Image of the laser-induced fluorescence and chemiluminescence of K atoms in the hot flue gas produced by a fuel-rich flame above the burner.

Figure 3.13
Voltage of photodiodes as a function of laser frequency without (a) and with (b) KOH seeding in the 404.4 nm TDLAS system. The potassium concentration in the case with KOH seeding was calculated to be 1.64 ppm. The voltage of etalon was shown in (a).

However, as the concentration of K atoms increased to several ppm, an optically thick condition resulting in saturated absorption was observed as reported by Qu et al.[25], especially in the present burner with a long optical path length. Figure 3.12 shows the laser-induced fluorescence of K atoms excited by the 769.9 nm laser under a fuel-rich condition. In the fuel-rich condition, several ppm K atoms can be generated [15]. In the image, the laser beam entered the hot flue gas from the left side, and almost no fluorescence could be observed in the right part of the hot flue gas. It indicates that the light was almost completely absorbed by the K atoms in the hot flue gas.

Due to the fact that the Einstein spontaneous emission coefficient of the 404.4 nm line is ~30 times smaller than the one of 769.9 nm line [27], the 404.4 nm line has a much smaller absorption cross section, which allows for measurements of higher K atom

concentration without saturation effects. A TDLAS system at 404.4 nm was developed in the present work to measure the concentration of K atoms at ppm-level. The TDLAS system at 404.4 nm is almost the same as the one at 769.9 nm. An external cavity laser (Toptica) was used to produce the beam with a wavelength of 404.4 nm probing the potassium $4^2S_{1/2} \rightarrow 5^2P_{3/2}$ transition. As shown in Figure 3.13 (a), the 404.4 nm TDLAS system had a scanning range of ~21 GHz, and the absorption is far from the optically thick condition even with a K atom concentration of 1.64 ppm as shown in Figure 2.13 (b). Further details, such as the fitting of the frequency dependent absorbance, and the absorption peak correction under optically thick conditions for even higher concentration measurement, can be found in Paper III.

3.4 KOH, KCl, SO₂ and OH measurement

Broadband UV absorption spectroscopy, also based on the Beer-Lambert law, was adopted for the measurement of concentrations of KOH, KCl, SO_2 and OH radicals in the hot flue gas. Similar to previous works [11, 28], a deuterium lamp was used as a broadband UV light source. The light provided by the lamp was collimated by a parabolic mirror to form a beam with a diameter of ~10 mm that passed above the burner six times using five UV-enhanced aluminium mirrors as shown in Figure 3.14. After the passages, the UV light was collected to a spectrometer (USB2000+, Ocean Optics) with a spectral resolution of ~0.3 nm.
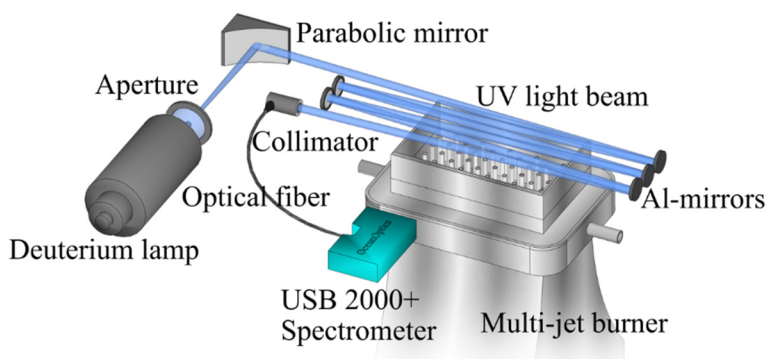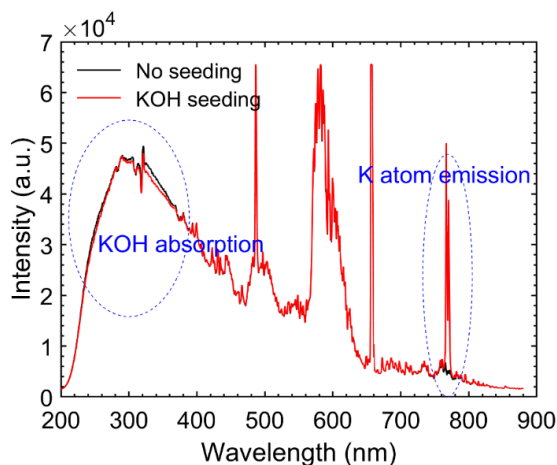

Figure 3.14
Schematic setup for the broadband UV absorption spectroscopy system.

In Figure 3.15, the red and black curves indicate the spectra of the UV light after the passage of the hot flue gas with and without KOH seeding, respectively. Comparing these two curves, the main differences are observed at the wavelengths around 300 nm

and 766/769 nm. In the hot flue gas with KOH seeding, K atoms were generated through the reaction KOH + H = K + H$_2$O, and the extra spectral lines at 766/769 nm are attributed to the strong chemiluminescence emission of K atoms. The reduction of the intensity at the wavelengths around 300 nm indicated by the dashed ellipse, was caused by the UV absorption of gas-phase KOH.

Figure 3.15
Spectra of the UV light after the passage of the hot flue gas with or without KOH seeding.

The absorbance, $A(\lambda)$, of alkali compounds, here mainly KOH and KCl, in the hot flue gas can be defined as:

$$A(\lambda) = -\ln\left(\frac{I_s(\lambda)}{I_0(\lambda)}\right) \qquad (3.6)$$

where $I_0(\lambda)$ and $I_s(\lambda)$ are the intensity of the UV light after the passage of the hot flue gas without and with KOH/KCl seeding, respectively. A typical absorbance curve of KOH obtained in the experiment is presented in Figure 3.16 (a). Using the absorbance of KOH or KCl, the concentration can be calculated based on the Beer-Lambert law:

$$A(\lambda) = N_A \cdot \sigma_A(\lambda) \cdot L \qquad (3.7)$$

where N_A is the number density, $\sigma_A(\lambda)$ is the absorption cross section of the alkali species, and L is the absorption path length. Unfortunately, the UV absorption cross sections of both gas-phase KOH and KCl at temperatures above 1100 K were unknown. Hence, in the present work, measuring the UV absorption cross sections of KOH and KCl accurately at high temperature became a crucial issue. Davidovits et al.

[29] and Leffler et al. [28] have measured the UV absorption cross sections of KCl at ~1000 K using a quartz cell with alkali chloride vapour. However, through this apparatus, it is hard to reach a higher temperature to mimic the combustion atmosphere. In the present work, as reported in Paper III, a new method was developed to measure the UV absorption cross sections of KOH and KCl at the temperature between 1300 K and 1800 K in the multi-jet burner.
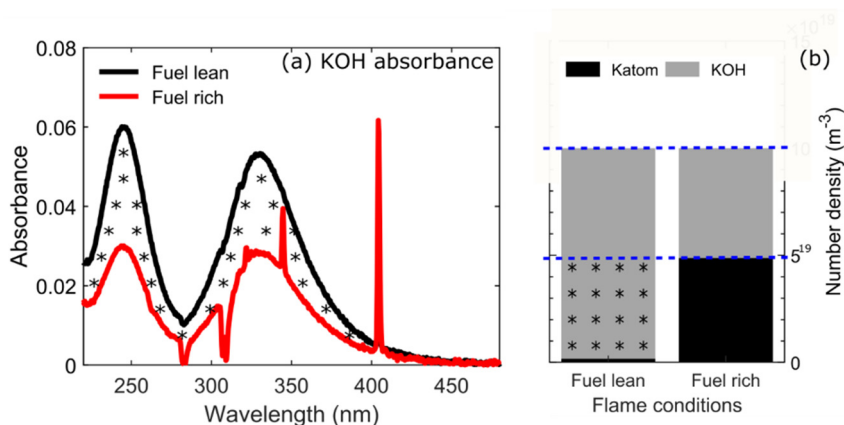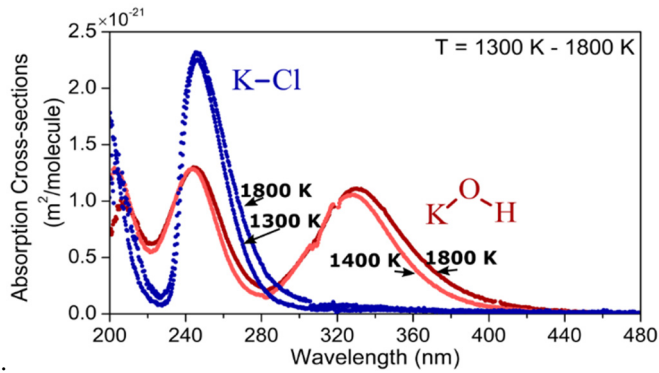

Figure 3.16
Absorbance of KOH in the fuel lean and rich cases (a) and corresponding number density of K atoms (b) in the hot flue gas.

As shown in Figure 3.16 (a), the absorbance of KOH in the hot flue gas provided by the fuel-rich flame T2O5 (T = 1840 K, ϕ = 1.12) was significantly weaker than the one in the flue gas provided by the fuel-lean flame T2O1 (T = 1770 K, ϕ = 0.67), despite that same amount of KOH was introduced in both cases, and these two cases had similar temperature. According to the potassium chemistry, KOH and K atoms should be the dominant potassium species under these two conditions, but the balance between KOH and K atoms could be significantly different. This was observed in the experimental measurement on K atom concentration using TDLAS system. As shown in Figure 3.16 (b), the number density of K atoms was 1.7×10^{18} m^{-3} and 4.87×10^{19} m^{-3} in the fuel-lean and fuel-rich case, respectively. It means that KOH was the dominant potassium species in the fuel-lean case, but in the fuel-rich case, a considerable amount of KOH was converted into K atoms. The part of KOH that was converted into K atoms had the absorbance equalling to the difference between the absorbance of KOH in the fuel-lean and the one in the fuel-rich case as shown in Figure 3.16 (a), which was marked with scatter star. Hence, the absorption cross sections of KOH were obtained using the Beer-Lambert law,

$$\Delta A_{KOH}(\lambda) = \Delta N_{KOH} \cdot \sigma_{KOH}(\lambda) \cdot L \qquad (3.8)$$

where ΔA_{KOH} and ΔN_{KOH} are the changes in absorbance and number density of KOH as the hot flue gas case varied from the fuel-lean to the fuel-rich, respectively. The obtained UV absorption cross sections of KOH are presented in Figure 3.17. Using the absorption cross sections, the concentration of KOH in the fuel lean case was calculated to be around ~20 ppm. In addition, ~100 ppm of Cl was introduced into the KOH seeded fuel-lean flue gas, and almost all the KOH was converted into KCl. Through the comparison between the absorbance spectrum of KOH and KCl, the UV absorption cross sections of KCl were measured as shown in Figure 3.17. It is also possible to obtain the UV absorption cross sections of NaCl and NaOH based on the cross sections of KOH using the method described by Weng et al. [30].
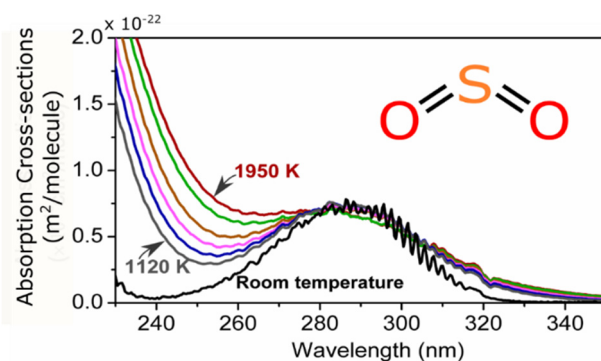

Figure 3.17
UV absorption cross sections of KOH and KCl at temperature of 1300 K and 1800 K.
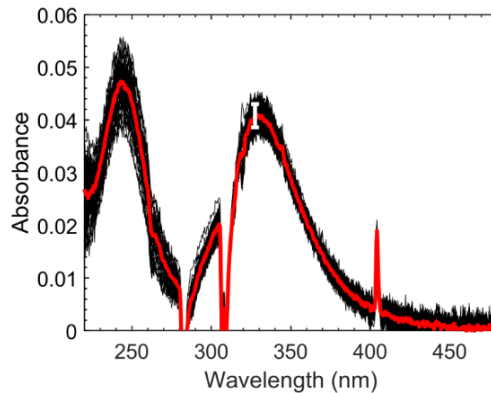
Figure 3.18
Absorbance of KOH in the hot flue gas under 50 measurements (black lines) and the average value (red line).

44

According to the measured absorption cross sections of KOH and KCl at different temperatures, it can be seen that the influence of the temperature on the cross sections is small, which has been reported by Leffler et al. [28]. However, the difference between the spectrum of KOH and KCl is significant, especially at wavelengths around 330 nm. This difference is beneficial for the distinction of KCl from KOH when both of them exist in the hot flue gas.

The measurement sensitivity of the broadband UV absorption spectroscopy system was evaluated based on the standard deviation of the absorbance with 50 measurements, as shown in Figure 3.18. Referencing to the random scattering of the absorbance observed at the wavelengths without any absorption, the sensitivity of the system was estimated to be about ~2 ppm.

Figure 3.19
UV absorption cross sections of SO_2 at varying temperatures up to 1950 K obtained in the hot flue gas environments.

The UV absorption cross section of SO_2 has attracted many experimental studies [31-34]. However, accurate measurement at a temperature over 1100 K was still lacking. Since the absorption cross section of SO_2 is strongly influenced by temperature, having reliable measurements at different temperatures is necessary. In the present work, in Paper IV, the absorption cross section of SO_2 in combustion environments was investigated using our broadband UV absorption spectroscopic system and the multi-jet burner. Since SO_2 could be introduced into the hot flue gas with a known concentration, it became much easier to evaluate the absorption cross sections of SO_2 compared to KOH and KCl. SO_2 (1% in N_2) was mixed with the jet-flow and seeded into the hot flue gas at different temperatures. The spectrally resolved absorbance of SO_2 was obtained as the natural logarithm of the ratio between the intensity of the UV light after the passage of the hot flue gas with SO_2 seeding and the one without SO_2 seeding (cf. Equation 3.6). Based on the Beer-Lambert law (cf., Equation 3.7), the UV absorption cross section of SO_2 between 230 nm and 350 nm at temperatures varying
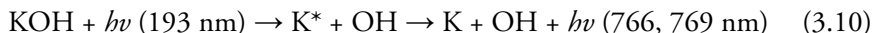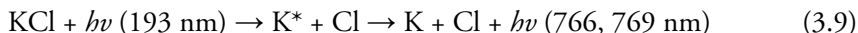
between 1120 K and 1950 K was measured. The results are presented in Figure 3.19. The values are almost 10 times smaller than the absorption cross sections of KOH and KCl shown in Figure 3.17, and they are very sensitive to temperature. The absorption cross section of SO_2 at wavelengths shorter than ~270 nm increases with temperature significantly. Hence, with spectrally resolved absorbance, not only reliable SO_2 concentrations can be obtained, the gas environment temperature can also be evaluated, as reported by Gao et al. [35].
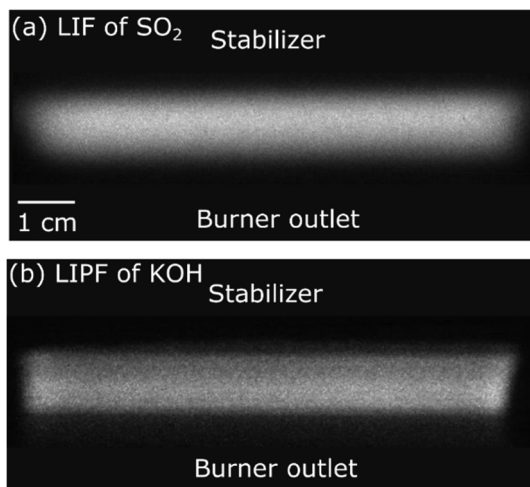
Figure 3.20
LIF signal of SO_2 (a) and LIPF signal of KOH (b) in the hot flue gas with an excitation by an 266 nm laser.

In order to measure the distribution of KOH and SO_2 in the hot flue gas, laser-induced photofragmentation fluorescence (LIPF) and laser-induced fluorescence (LIF) were adopted, respectively. The schematic of the experimental setup is presented in Paper IV. The fourth harmonic of a Nd:YAG laser was used to provide a 266 nm laser with a pulse energy of about 28 mJ/pulse. The laser beam was passed through the hot flue gas to directly excite SO_2 molecules. During the relaxation of the excited SO_2 molecules to the ground state, broadband UV fluorescence was generated. The spectrum of the fluorescence from 240 nm to 380 nm was recorded by a spectrometer, and it is presented in Paper IV. In order to have two-dimensional images of the fluorescence, the fluorescence was also collected by an ICCD camera through a long pass filter (Schott WG305). Figure 3.20 (a) presents a typical image of the SO_2 LIF signal in the hot flue gas. It can be seen that the distribution along the horizontal direction is quite uniform. As described in Paper IV, the fluorescence signal can be used to measure the concentration of SO_2 after calibration, and it shows that the LIF method was more sensitive than the broadband UV absorption spectroscopy method.

In the previous works reported by Leffler et al. [15, 36], two dimensional laser-induced photofragmentation fluorescence was adopted for the measurement of the distribution of KOH and KCl in the hot flue gas. An ArF Excimer laser was used to provide the 193 nm laser to photodissociate gas-phase KOH and KCl molecules as,

$$KCl + h\nu \text{ (193 nm)} \rightarrow K^* + Cl \rightarrow K + Cl + h\nu \text{ (766, 769 nm)} \tag{3.9}$$

$$KOH + h\nu \text{ (193 nm)} \rightarrow K^* + OH \rightarrow K + OH + h\nu \text{ (766, 769 nm)} \tag{3.10}$$

and electronically excited K atoms (K*) were generated. When the exited K atoms relaxed to the ground state, fluorescence at 766 nm and 769 nm was generated [36]. The resulting fluorescence can be collected for concentration evaluation. However, the laser at 193 nm photodissociated both KOH and KCl, which made it hard to distinguish them from each other when both KOH and KCl existed in the hot flue gas.

It has been reported by Oldenborg and Baughcum [37] that almost no excited K atoms could be generated as gas-phase KCl was photodissociated by light at 266 nm. However, it is still not clear whether excited K atoms could be generated from KOH via photodissociation by the 266 nm laser. In the present work, a laser beam provided by the fourth harmonic of a Nd:YAG laser with a wavelength at 266 nm was formed into a laser sheet with two cylindrical lenses. When the laser passed through the hot flue gas containing gas-phase KOH, fluorescence at 766/769 nm was detected by an ICCD camera with an interference band pass filter at 766 nm with a FWHM of 10 nm. It indicates that, when KOH absorbed the photons at 266 nm, it was not only dissociated into ground state K atoms [38], but also into exited K atoms. During the relaxation of the exited K atoms to the ground state, fluorescence was emitted. A typical image of the fluorescence signal in the hot flue gas is shown in Figure 3.20 (b). Based on the fluorescence signal, the distribution of KOH concentration can be obtained after calibration. Combining the LIPF technique using a 193 nm laser as reported in the previous work [36] and the 266 nm laser in the present work, two-dimensional measurements on KOH and KCl concentration with species distinction can be achieved.

In the present work, as a preliminary investigation, the LIPF technique at 266 nm was applied for a study of the release of KOH from burning biomass pellets. A straw pellet was placed above the burner using two ceramic holders (cf. Figure 3.21 (a)) and burned in the hot flue gas (cf. Figure 3.21 (b)). The 266 nm laser sheet passed above the burning straw pellet, and the fluorescence at 766/769 nm was captured representing the distribution of KOH released from the burning pellet. It can be seen that gas-phase KOH was formed at ~2 mm downstream of the surface of the pellet during its char

burning stage. In the layer close to the surface of the pellets, K atoms can be the dominant potassium species.

Moreover, through the KOH LIPF technique and SO_2 LIF technique, the distribution of KOH and SO_2 in the counter-flow reactor discussed in Chapter 2 can be obtained for further K-Cl-S chemistry investigations.
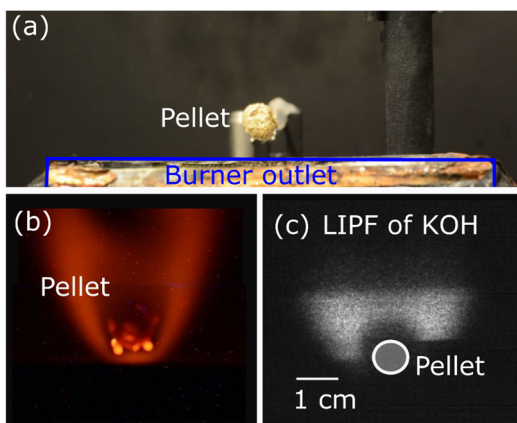
Figure 3.21
Photos of a pellet above the burner (a) and its char burning (b), and the LIPF signal of KOH surrounding the burning pellet (c).
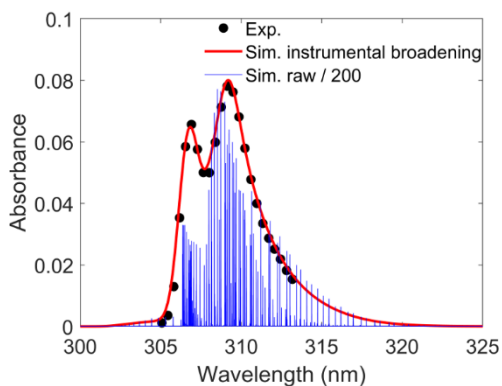
Figure 3.22
Absorbance of OH measured in the hot flue gas and its simulation at 500 ppm with or without including instrumental broadening effect.

OH radicals absorb UV light at wavelengths around 310 nm. Using broadband UV absorption spectroscopy, Gao [39] has achieved measurement of the absolute OH number density in a Bunsen-type premixed flame. In the present broadband UV

absorption system for KOH, KCl and SO_2 measurements, information related to the absorption of OH radicals at around 310 nm was also extracted. As shown in Figure 3.18, a dip around 310 nm appeared. This is because that the concentration of OH radicals in the hot flue gas decreased with KOH seeding.

In the OH radical measurement, the absorbance of OH radials was obtained based on the natural logarithm of the ratio between the intensity of the light after and before passing through the hot flue gas. The typical absorbance of OH radicals in the hot flue gas from flame T2O4 (T = 1790 K, ϕ = 0.96) is shown in Figure 3.22 with black dots. In order to fit the simulated OH absorption spectrum from LIFBASE [40] (cf. blue lines in Figure 3.22) to the measured one, convolution processing was conducted taking the instrumental broadening into account. The simulated spectrum for a concentration of 500 ppm (cf. red line in Figure 3.22) can be well fitted to the absorbance obtained in the experiment.

Chapter 4

Quantitative K-Cl-S chemistry

Gas-phase K-Cl-S chemistry was investigated in the homogenous hot gas environments provided by the multi-jet burner. The hot gas environments had a temperature varying between 1120 K and 1950 K. Potassium, chlorine, and sulfur was homogeneously introduced into the hot flue gas. The concentrations of KOH, KCl, K atoms, SO_2, and OH radical were measured using broadband UV absorption spectroscopy and tunable diode laser absorption spectroscopy (TDLAS). Simulation were conducted in Chemkin-Pro [16] with a detailed K-Cl-S mechanism to predict the experimental results.

4.1 Experimental measurements

In the present work, the investigation was conducted on the KOH-, KCl- and SO_2-doped hot gas products provided by the multi-jet burner as shown in Figure 4.1. Small droplets in the fog of K_2CO_3/KCl water solution generated by an ultrasonic fog generator passed through the premixed jet flames and converted into gas-phase KOH and KCl. SO_2 was seeded into the hot flue gas by mixing into the co-flow.

The detailed structure of the burner head is shown in Figure 4.1. The flow stabilizer was ~35 mm above the burner outlet, and the burner outlet was ~29 mm or ~17 mm above the premixed flame fronts. Here, two types of flames were adopted: lifted ones and attached ones. The lifted flames were adopted in the high-temperature cases (above 1700 K), which reduced the heat loss to the burner jets, but for the low-temperature conditions (below 1700 K), attached flames were much easier to stabilize on the jets.

Moreover, attached flames can ensure that all the salt passes through the flame fronts and is completely vaporized quickly. All the flame conditions used in the present work are presented in Table 3.1.
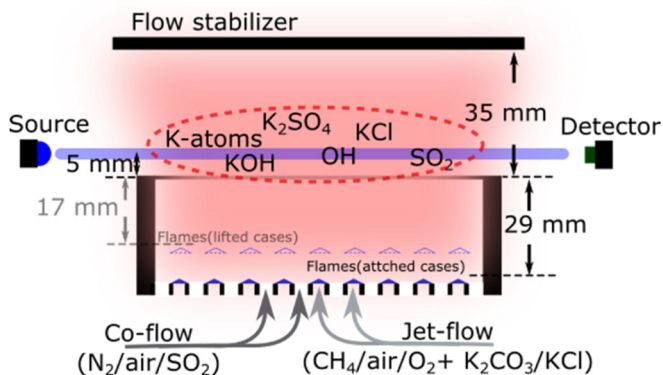
Figure 4.1
Detail of the multi-jet burner head with hot flue gas products containing potassium, chlorine and sulfur, and a schematic of the absorption spectroscopy technique.
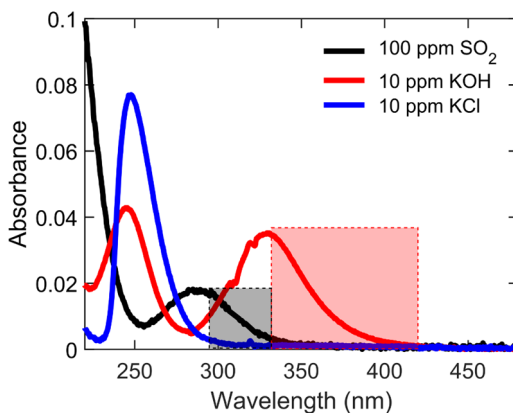
Figure 4.2
Absorbance of KOH, KCl and SO$_2$ in the hot flue gas at temperature 1260 K.

The concentrations of KOH, KCl, SO$_2$ and OH radicals were quantitatively measured simultaneously using our broadband UV absorption spectroscopy system, the K atom concentration was measured using the TDLAS system, and the temperature was obtained using the TLAF thermometry with indium atoms, as described in detail in Chapter 3. All the measurements were conducted at a height of ~5 mm above the outlet of the burner, as shown in Figure 4.1.

Spectrally resolved absorbance of KOH, KCl and SO_2 at wavelengths from 220 nm to 480 nm are presented in Figure 4.2. The overlap of these UV absorption spectra was the main challenge in concentration measurements. Fortunately, at wavelengths longer than ~330 nm, only KOH has absorption, and, thus, based on the UV absorption at these wavelengths, the concentration of KOH can be evaluated. The rest part of the absorbance without any contribution from KOH, can be separated into the absorbance of KCl and SO_2, based on the absorption at wavelengths over ~300 nm where the absorption was mainly attributed to SO_2. In principle, the spectrally resolved absorption cross section curves belonging to KOH, KCl and SO_2 have distinct shapes which can be used to fit the measured spectra containing different species to a linear combination of contributions from different species to obtain unambiguous concentrations.

4.2 Modelling work

Simulation work was conducted using Chemkin Pro [16]. A one-dimensional stagnation reactor, mimicking the experimental conditions, was used to simulate the reactions occurring along the vertical axial in the centre of the burner as shown in Figure 4.3. The mixtures of the co-flow and the gas products from the jet-flames were used as the inlet gas of the model. Here, the gas products of the jet-flames were obtained using a one-dimensional free propagation premixed flame model in Chemkin Pro [16] with the GRI-3.0 mechanism [17]. The concentrations of KOH/KCl mixed in the gas inlet was set to be the one measured in the flue gas products. The temperatures along the axial direction in the model (cf. Figure 4.4) were assigned to be the ones measured by a type B thermocouple at different positions along the vertical axis. The measured temperatures were corrected using heat-transfer theory considering that heat losses occurred in the thermocouple through thermal radiation. The axial distance in the model was set to be 52 mm and 64 mm for the cases that adopted lifted flames and attached flames, respectively, which was the distance between the flame fronts and the flow stabilizer as shown in Figure 4.1.

Figure 4.4 presents typical distributions of temperature and concentrations of KOH, K atoms and OH radicals along the vertical axis obtained through the simulation. In the simulation, the hot gas products from flame T2O4 (T = 1790 K, ф = 0.96) and T2O5 (T = 1840 K, ф = 1.12) were used, and 20 ppm KOH was introduced. Under the oxidizing condition, KOH was the dominant potassium species, while under the reducing condition, abundant K atoms were generated. The concentrations of K atoms and OH radicals decrease with the vertical height, which represents the reaction time

of the gas products. This phenomena has been obsrved by Slack et al. [14] experimentally. The significant reduction in OH concentration can be caused by the temperature decrease and the chain-terminating reaction K + OH + M = KOH + M. At the measurement height (marked with black dot line in Figure 4.4), the species concentrations in fuel-lean case show to be closer to chemical equilibrium values than the ones in fuel-rich case.
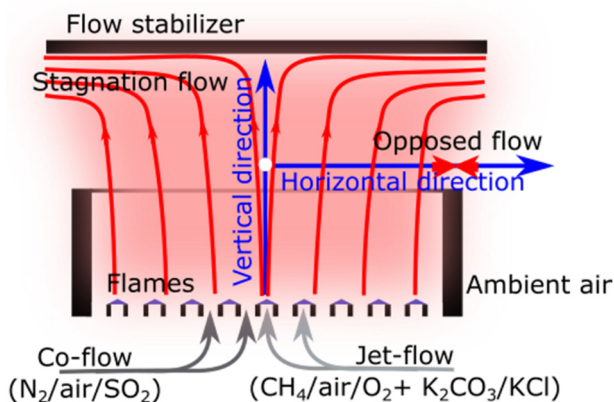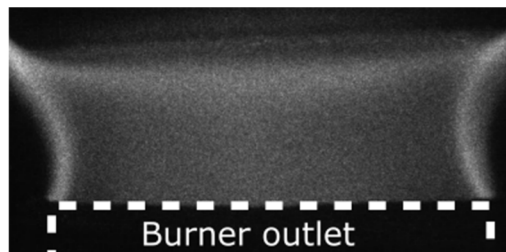

Figure 4.3
Schematic of the burner head and flow field for the simulation using Chemkin software.
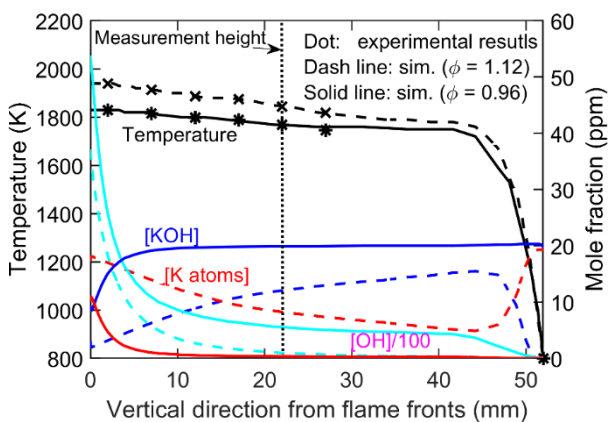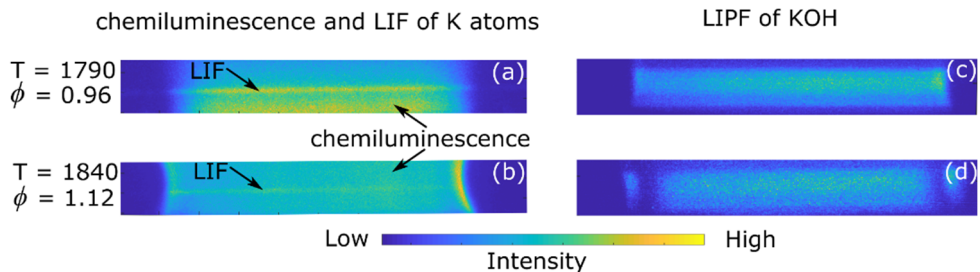

Figure 4.4
Distribution of the temperature and the concentrations of KOH, K atoms and OH radicals along the vertical direction in the hot flue gas.

Even though the distribution of the concentrations in the hot flue gas is quite homogenous, on the edge of the hot flue gas, the concentrations can be different from the central part due to edge effects. For example, in the fuel rich cases, diffusion flames were formed as the flue gas met the ambient air due to the oxidation of CO and H_2 from the hot flue gas. As shown in Figure 4.5, chemiluminescence at 430 nm was obtained in the fuel-rich case by an ICCD camera. The chemiluminescence at 430 nm raised from CO_2^* from the CO oxidation. The flame front of the diffusion flame on the edge can be clearly observed. In the experiment, the concentrations are the average values along the measurement path as shown in Figure 4.1, which included the edge effect. However, the simulation with the one-dimensional stagnation reactor only predicted concentrations of the species at the centre of the flue gas as shown in Figure 4.3.

Figure 4.5
Chemiluminescence at 430 nm obtained in the fuel-rich case raised from the oxidation of CO.

Figure 4.6
LIF signal of K atoms and LIPF signal of KOH in both oxidizing and reducing cases with ~20 ppm KOH seeding.

The edge effect introduced an uneven distribution of the species along the horizontal direction. There are two ways to solve the problem caused by the edge effect. One is correcting measurement results to obtain the concentrations in the centre of the hot flue gas, and the other one is improving the simulation process to include the edge part.

As reported in Chapter 3, the distribution of the key species can be obtained using laser-induced fluorescence or laser-induced photofragmentation fluorescence. Combining LIF or LIPF with broadband UV absorption spectroscopy, the quantitative concentration distribution of those key species can be measured. In the present work, K atoms were excited by a continuous wave laser at 769.9 nm, and the resulting resonance fluorescence was recorded by an ICCD camera with an interference band pass filter at 766 nm. Figure 4.6 (a) and (b) presents the distribution of the K atom LIF signal together with the chemiluminescence of K atom. Gas-phase KOH was photodissociated by a 266 nm laser sheet as described in Chapter 3. The LIPF signal of KOH was obtained and its distribution is shown in Figure 4.6 (c) and (d).

However, the signal distribution presented in Figure 4.6 cannot represent the distribution of the fluorescence in the probe volume, since part of the LIF and LIPF signal was trapped by the K atoms in the hot flue gas, which has been reported by Leffler et al. [36]. As shown in Figure 4.6 (d), in the region close to the edge of the hot flue gas, the disappearance of the signal can be caused by the high concentration of K atoms there. Without accurate concentration measurement of the K atoms on the edge, the correction on the fluorescence may contain a big uncertainty, and it is hard to obtain a reliable measurement on the potassium species distribution on the edge.

In the present work, the second method was adopted. As described in Paper V, the opposed-flow model in Chemkin-Pro [16] was used to simulate the reaction process occurring along the horizontal axial in the edge region at the measurement height as marked in Figure 4.3. Through this model, the concentration distribution of KOH, KCl, K atoms and OH radicals in the edge region was predicted.

The hot flue gas from the centre was used as one of the inlets of the opposed-flow model. The gas compositions and the temperature there was set to be the ones calculated by the stagnation model. The ambient air was used as the other inlet of the opposed-flow model, having a temperature of 298 K. The speeds of the hot flue gas and the air, and the distance between these two inlets were adjusted to make the simulated temperature and OH radical distribution close to the one obtained in experiment. In the experiment, the temperate distribution at the edge was obtained using two-line atomic fluorescence thermometry, and the OH radical distribution was represented by the distribution of the chemiluminescence signal at 430 nm considering that the signal raised from CO_2^* after the CO oxidation and the reaction CO + OH = CO_2 + H was the main oxidation path of CO. In the present work, when the speed of the hot flue gas and the ambient air was set to be 30 cm/s and 0.5 cm/s, respectively, and the axial distance was 1.5 cm, a good fitting was obtained as shown in Paper V. For a further investigation in the future, measurement of the velocity field at the edge

of the hot flue gas using particle image velocimetry (PIV) could definitely improve the accuracy of the simulation work.

When the horizontal concentration profiles of the potassium species and OH radicals were obtained in the simulation, the concentration was integrated and averaged with a hot flue gas size of 85 mm. The simulated results were compared with the experimental results directly as presented in Paper V and VI under different conditions to understand the K-Cl-S chemistry and evaluated the K-Cl-S mechanism. Paper V mainly focused on the K-Cl chemistry in both oxidizing and reducing environments with varying temperature; Paper VI mainly focused on the sulfation of KCl and KOH based on K-Cl-S chemistry; and Paper VII demonstrated the influence of potassium on the oxidation of CO and H_2.

4.3 Results and discussion

Paper V provides unprecedented quantitative experimental data of KOH, KCl, K atoms and OH radicals under the conditions with a wide variation in the potassium adding concentration, the fuel-air equivalence ratio, and the gas environment temperature for the study of K-Cl chemistry.
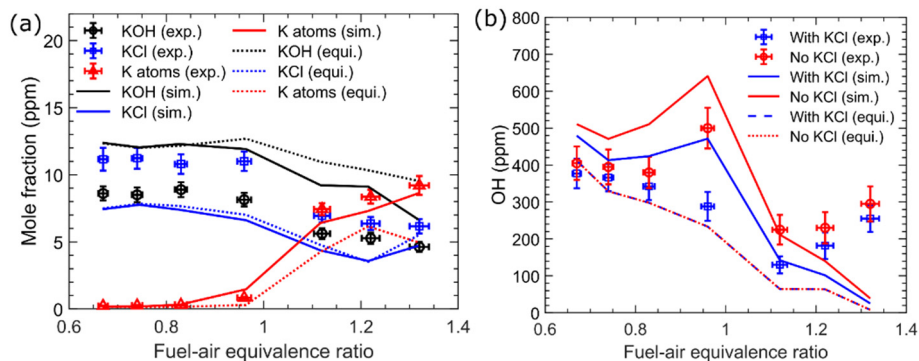
Figure 4.7
Concentrations of KOH, KCl, K atoms (a) and OH radicals (b) in the hot flue gas at ~1800 K provided by flames T2O1-T2O7 with varying global equivalence ratios with about 20 ppm potassium seeding from KCl. Experimental results are indicated with symbols with error bars, simulation results from stagnation model are indicated with solid lines and the ones from equilibrium calculation are indicated with dash lines.

In the first part, the effect of the variation in potassium seeding concentration was investigated. Different amounts of K_2CO_3 were introduced in the hot flue gas from flame T2O5 (T = 1840 K, ϕ = 1.12). It was found that K_2CO_3 was converted into

KOH and K atoms in roughly equal amounts. Both concentrations of KOH and K atoms increased almost linearly with the total potassium seeding amount. When KCl was introduced in the flame, the measured concentration of KCl, KOH and K atoms were of the same order, and they increased almost linearly with total potassium concentration. A reasonable agreement between the results from experiments and simulations was obtained.

In the second part, the effect of equivalence ratio was studied. For both K_2CO_3 and KCl seeding, a significant increase in the concentration of K atoms was observed when the fuel-air equivalence ratio varied from lean to rich conditions. As shown in Figure 4.7 (a), when ~20 ppm of KCl was introduced into the hot flue gas, the concentration of K atoms increased from negligible in the lean flames to become the most abundant potassium component, over 8 ppm, under reducing conditions. The results from the simulation have similar trends, as shown in Figure 4.7. Besides the simulation based on the stagnation flow model, some calculations were also conducted using the equilibrium model in Chemkin-Pro to have the chemical equilibrium analysis. The divergence between the simulation from these two models under rich conditions indicates that it takes longer time for the potassium in reducing environments to reach chemical equilibrium than the one in oxidizing environments. The variation in the OH radical concentration in the hot flue gas with and without 20 ppm KCl seeding as a function of equivalence ratio is shown in Figure 4.7 (b). The concentration of OH radical was reduced significantly for the cases near the stoichiometric condition, and it can be found that the experimental results with potassium seeding was quite close to chemical equilibrium, being different from the simulation results based on the stagnation flow model.

Finally, the measurements of the concentrations of KOH, KCl and K atoms in the hot flue gas at different temperatures were conducted, as presented in Paper V. In the gas environment with a higher temperature, more K atoms were detected, and more KOH was converted from KCl.

The investigation of K-Cl-S chemistry mainly focused on the sulfation process occurring between KCl/KOH and SO_2, as presented in Paper VI. Based on the measurement of the concentrations of KCl, KOH and K atoms, it can be found that KOH was sulfated more rapidly than KCl, since more K atoms were generated in the hot flue gas with KOH seeding than the one with KCl seeding. As reported in Chapter 2, atomic K produced in the hot flue gas is one of the key species in sulfation reactions according to the sulfation reaction pathway. The concentration of K atoms in the ~20 ppm KOH seeded hot flue gas from flame T6O2 (T = 1120 K, ϕ = 0.6) with a temperature of 1120 K was measured to be ~10 ppb, while the ~20 ppm KCl seeded hot flue gas had only ~0.15 ppb of K atoms. Almost all the ~20 ppm KOH was sulfated

by the 150 ppm SO_2, while only ~25% of ~20 ppm KCl was sulfated. Moreover, it was found that the sulfation was more significant for the cases with a lower temperature. As shown in Figure 4.8, almost no sulfation occurred as the temperature reached ~1550 K. All these phenomena can be well predicted by the simulation based on the detailed K-Cl-S mechanism.
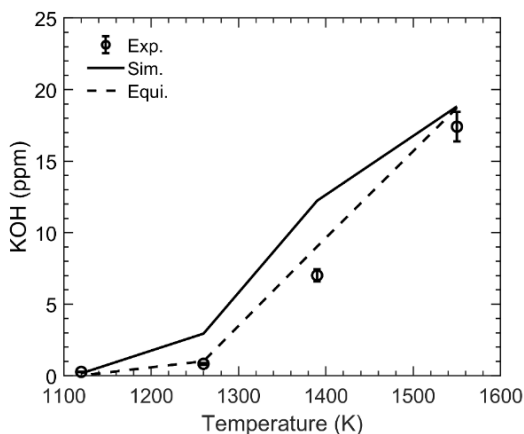
Figure 4.8
Concentration of KOH remained in the hot flue gas from the flame (T3O2 - T6O2) with mixing of 20 ppm KOH and 150 ppm SO_2. Experimental results are indicated with symbols with error bars, simulation results from stagnation model are indicated with solid lines and the ones from equilibrium calculation are indicated with dash lines.
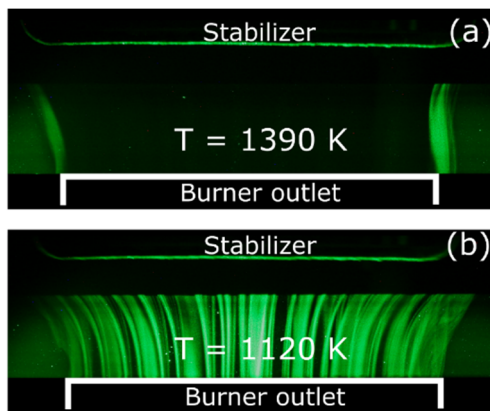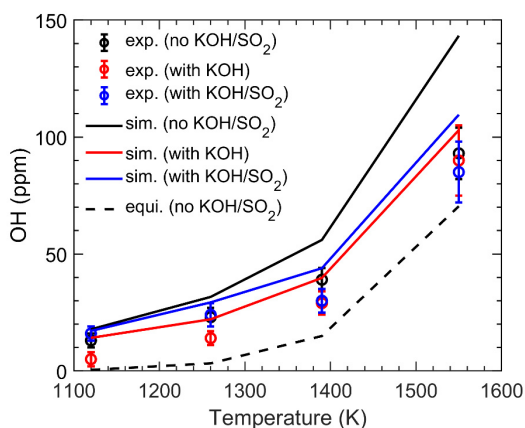

Figure 4.9
Mie scattering signal from aerosols in the hot flue gas from the flame T4O2 (T = 1390 K, ϕ = 0.67) and T6O2 (T = 1120 K, ϕ = 0.6) with 20 ppm KOH and 150 ppm SO_2.

According to the observation based on the light scattering in the hot flue gas at a low temperature, such as 1120 K, as shown in Figure 4.9 (b), the consumed KOH was partly transformed into condensed K_2SO_4 aerosols. However, at the temperature of 1390 K, even though more than half of KOH was consumed (cf. Figure 4.8), no K_2SO_4 aerosols were observed. This indicates that gas-phase potassium-sulfur compounds were formed in the hot flue gas, mostly $KHSO_4$ and K_2SO_4 as predicted in the simulation.

Figure 4.10 presents the variation in the concentration of OH radicals in the hot flue gas with or without KOH/SO_2 seeding. Corresponding results are also presented in Paper VI. The OH concentration significantly increased with temperature. It was marginally affected by the SO_2 seeding, but reduced with KOH seeding. The reduction is mainly caused by the chain terminating reaction sequence $KOH + H = K + H_2O$, and $K + OH + M = KOH + M$. When strong sulfation occurred in the low temperature cases with seeding both KOH and SO_2, the terminating reaction sequence was eliminated and more OH radicals survived. The simulation results show reasonable agreement with the experimental results.
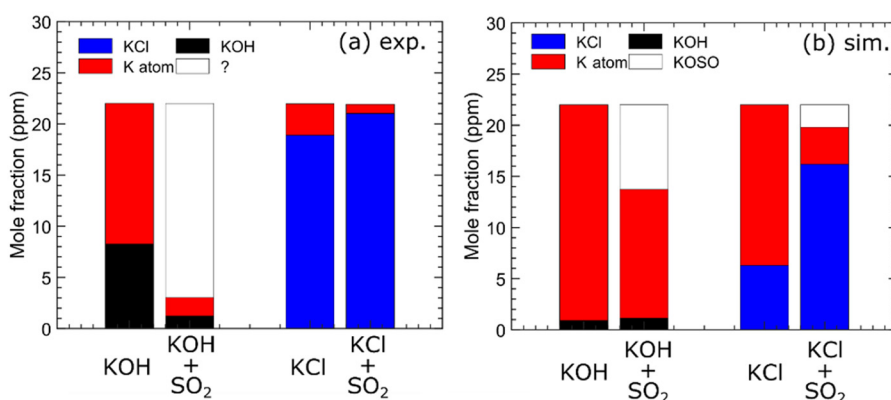

Figure 4.10
Concentration of OH radicals in the hot flue gas from the flame (T3O2 - T6O2) with or without seeding 20 ppm KOH or 150 ppm SO_2. Experimental results are indicated with symbols with error bars, simulation results from stagnation model are indicated with solid lines and the ones from equilibrium calculation are indicated with dash lines.

The sulfation process in a reducing hot gas environment was also quantitatively investigated. It was the first time that the detailed K-Cl-S mechanism was evaluated in a reducing gas environment. The details are presented and discussed in Paper VI. The concentrations of KOH, KCl and K atoms were measured in a reducing hot gas environment provided by flame T6O7 (T = 1140 K, = 1.31) with a temperature of 1140 K and with 22 ppm KOH or KCl seeding. The results are shown in Figure 4.11

(a). About 15 ppm K atoms were generated in the KOH-seeded hot flue gas, while only ~4 ppm K atoms were generated in the KCl seeded one. When 150 ppm SO_2 was added into the KOH seeded hot flue gas, the concentrations of KOH and K atoms were dramatically decreased, and some species with extra spectra distinguished from KOH and SO_2 were observed, as presented in Paper VI. The unknown absorption spectrum was attributed to KOSO according to the predictions based on K-S chemistry in a reducing environment, as shown in Figure 4.11 (b). KOSO was formed through the reaction $K + SO_2 = KOSO$. Due to the absence of O_2 in the reducing environment, KOSO was not further transformed into K_2SO_4. This reaction was much weaker in the KCl seeded hot flue gas. Especially according to the observation in our experiment, no potassium was converted into KOSO from KCl.

Figure 4.11
Concentrations of KOH, KCl and K atoms in the hot flue gas from flame T6O7 (T = 1140 K, ϕ = 1.31) with introducing 22 ppm KOH/KCl and 150 ppm SO_2, obtained from experiment (a) and simulation (b).

In Paper VII, the influence of potassium on CO and H_2 oxidation in combustion environments was studied. Typical results are shown in Figure 4.12. Being different from measurements of the concentrations of K atoms and OH radicals by optical methods, the concentrations of CO and H_2 in the hot flue gas were measured using a micro-gas chromatograph (GC) system. The gas at the measurement height 5 mm above the burner outlet was extracted by a sampling tube made by stainless steel, and collected in a gas bag with a volume of ~300 mL with the help of a syringe. The gas was cooled down, filtered, and dried before entering the bag. The GC system took gas sample from the gas bag, and analysed the gas composition. Since the obtained results were the concentrations in the dried gas, the results were corrected to the concentration in the hot flue gas based on the concentration of H_2O there, that was estimated based on chemical equilibrium.
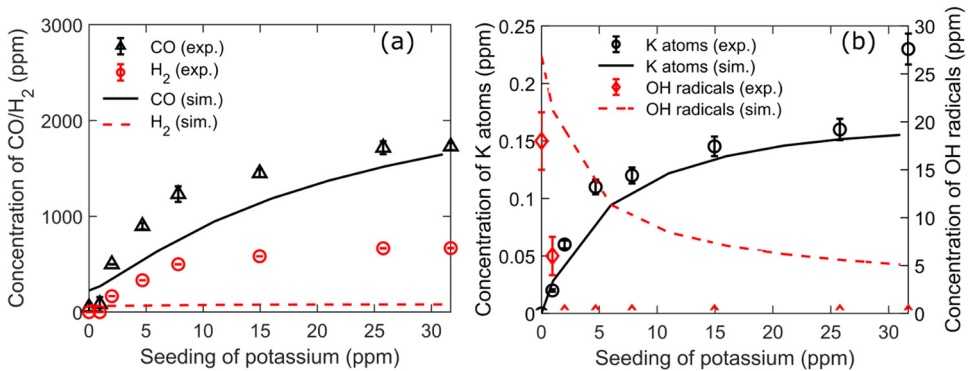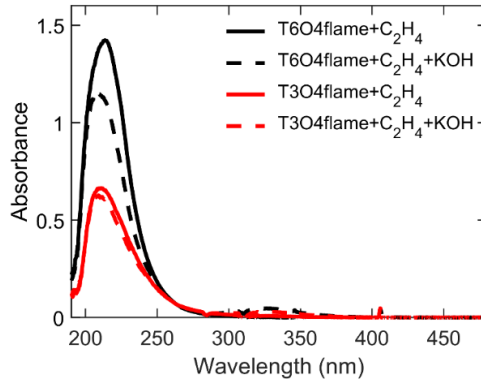
Figure 4.12
Concentrations of CO, H₂, K atoms and OH radicals in the hot flue gas from flame T6O4 (T = 1120 K, φ = 0.96) with introducing different amounts of KOH. Experimental results are indicated with symbols with error bars, and simulation results from stagnation model are indicated with lines.

In Figure 4.12, the hot gas environment was provided by flame T6O4 (T = 1120 K, φ = 0.96) with a temperature around 1120 K and oxygen concentration of ~0.5%. When KOH was introduced into the hot flue gas, the oxidation of CO and H_2 was inhibited. About 1800 ppm CO and 700 ppm H_2 remained in the hot flue gas with ~30 ppm KOH seeding, despite the fact that it was an oxidizing environment. Together with the increase in the concentrations of CO and H_2, the concentration of K atoms increased with total KOH seeding. The OH radials in the hot flue gas were consumed rapidly by the chain terminating reaction sequence KOH + H = K + H_2O, and K + OH + M = KOH + M as described above. The reduction of the concentration of OH radicals may direct affect the oxidation of CO and H_2. The simulation could well predict the phenomenon, but still some deviation existed, as the simulation underpredicted the concentration of H_2.

In Paper VII, it is also shown that in the hot flue gas at a higher temperature or having a lower fuel-air equivalence ratio, the influence from the potassium seeding on the oxidation of CO and H_2 could be much smaller. Almost no effect on the oxidation of CO and H_2 from potassium seeding was observed when the temperature reached 1550 K. At this temperature, certain amounts of OH radicals remained in the hot flue gas despite the enhanced OH consumption due to KOH seeding. Moreover, chlorine and sulfur adding in the hot flue gas also reduced the inhibiting effect of potassium on the oxidation of CO and H_2 due to the reduction in the concentrations of KOH and K atoms and resulting less consumption in OH radicals in the hot flue gas as shown in Figure 4.10.

Figure 4.13
Absorbance obtained in the hot flue gas environments provided by Flame T6O4 (T = 1120 K, ɸ = 0.96) and T3O4 (T = 1530 K, ɸ = 0.96) with 1.7% C_2H_4 and 20 ppm KOH seeding.

Additionally, some previous studies show that potassium may play an important role in the PAH conversion and tar formation, during the gasification of biomass fuels [41]. Thus, a preliminary study was conducted to investigate the effect of potassium on the pyrolysis of C_2H_4 and the formation of PAH in the hot gas environments provided by flame T6O4 (T = 1120 K, ɸ = 0.96) and flame T3O4 (T = 1530 K, = 0.96). When C_2H_4 was seeded into the hot flue gas together with co-flow with a concentration of ~1.7%, through the broadband UV absorption spectroscopy system, an absorption peak at the wavelength around 220 nm was observed, as shown in Figure 4.13. The absorption spectra may be contributed by the absorption of C_2H_2 [32] or light aromatics [42] which were converted from C_2H_4. As ~20 ppm KOH was introduced into the hot flue gas, the absorption of KOH around 320 nm could be observed clearly, and significant reduction of the absorbance at around 220 nm was obtained. This indicates that gas-phase KOH in the hot flue gas may influence the pyrolysis of C_2H_4 and formation of PAH at a relative low temperature, such as ~1120 K, through a homogenous reaction process. To clarify this process, further investigations are needed, such as PAH measurements using laser-induced fluorescence.

Chapter **5**

Summary and outlook

5.1 Summary

Preliminary investigation of the sulfation of KOH and KCl by SO_2 was conducted in a counter-flow reactor. The homogenous gas-phase sulfation between KOH/KCl and SO_2 occurred in oxidizing environment with consequent nucleation of K_2SO_4 at temperature between 1000 K and 1400 K. K_2SO_4 aerosols were observed as they were illuminated by a green laser sheet. KOH was more readily sulfated than KCl. Using an opposed-flow model in Chemkin-Pro, simulations were conducted with a detailed K-Cl-S mechanism and could predict the observation in the experiment. However, more quantitative measurements were desired for a better understanding of K-Cl-S chemistry and evaluation of the mechanism.

Hence, a laminar flame burner was designed to provide uniform hot gas environments for investigations of K-Cl-S chemistry. In the homogenous gas environment, absorption spectroscopy techniques could be applied for quantitative measurements of key species, such as KOH, KCl, K atoms, OH radicals and SO_2. The temperature of the hot gas environments was accurately measured using two-line atomic fluorescence (TLAF) thermometry, and the range of temperature covers from 1000 K to 2000 K.

In concentration measurements using absorption spectroscopy, an accurate absorption cross section is essential according to the Beer-Lambert law. For the first time, the UV absorption cross sections of KOH, KCl and SO_2 were obtained in combustion atmosphere. The absorption cross sections of KOH and KCl were marginally affected by temperature, while the one of SO_2 strongly depended on temperature.

The concentrations of KOH, KCl, SO₂ and OH radicals in the hot flue gas were monitored using broadband UV absorption spectroscopy at wavelengths between 220 nm and 480 nm. The concentration of K atoms was accurately measured using tunable diode laser absorption spectroscopy (TDLAS) at wavelengths 404.4 nm or 769.9 nm.

The experimental results show that in the oxidizing hot gas environments with KOH/KCl seeding, KOH and KCl are the dominant species. The balance between KOH and KCl strongly depends on the temperature. In the reducing environments, abundant K atoms were formed. When SO_2 was added into the KOH/KCl seeded oxidizing hot gas environment, potassium was sulfated as the temperature went below 1390 K. When the temperature was lower than 1260 K, K_2SO_4 aerosols was observed. In the reducing environments, KOSO was formed from the reaction between K and SO_2. KOH in the hot flue gas reduced the concentration of OH radicals due to a chain-terminating reaction sequence involving KOH, K atoms and OH radicals. The reduction of OH radicals can consequently limit the oxidation of CO and H_2.

Simulations were performed using stagnation and opposed-flow reactor modules in Chemkin-Pro. A detailed K-Cl-S chemical mechanism was adopted in the simulation and thus evaluated. A reasonable agreement between simulations and experimental results was obtained.

5.2 Outlook

In the present work, K-Cl-S chemistry in homogenously prepared hot gas environments was investigated through quantitative measurements using absorption spectroscopy. However, the measurements were only conducted at a certain height above the burner where chemical equilibrium was almost reached. In order to explore the whole chemical reaction process, further studies can be performed on a counter-flow reactor with spatially resolved quantitative measurements. Two-dimensional LIF and LIPF techniques can be employed. For example, the distribution of KOH/KCl can be obtained using the LIPF imaging technique. A laser beam at 193 nm provided by an Excimer laser can photodissociate both KOH/KCl, while the laser beam at 266 nm provided by the fourth harmonic of a Nd:YAG laser can photodissociate KOH only. SO_2 PLIF can provide the distribution of SO_2 with excitation by a 266 nm laser. However, the SO_2 fluorescence signal depends strongly on temperature. Thus, two-dimensional temperature measurements are also necessary. In Chapter 2, Rayleigh scattering was used for the temperature measurement. In order to have a temperature measurement with a higher accuracy, NO-LIF thermometry is proposed in a further study. Moreover, the distributions of K atoms and OH radicals can also be obtained

with corresponding planar-LIF technique. Combining the experimental results and the simulation work based on the opposed-flow model, the detailed K-Cl-S chemical mechanism can be further validated.

More homogeneous reactions involving potassium species can be further investigated in the multi-jet burner. As described in Chapter 4, preliminary investigation on the effect of potassium on the pyrolysis of C_2H_4 and the PAH formation was conducted. Further research can be made by monitoring PAH generation using different optical methods such as PAH-LIF or broadband UV absorption spectroscopy. The homogenous reactions involving other alkali compounds and nitrogen compounds can also be studied based on the quantitative measurements demonstrated in this thesis.

Not only homogeneous reactions, but also heterogeneous reactions can be studied in the burner. As presented in Paper II, single biomass pellets can be placed in the uniform hot flue gas, and their thermal conversion process can be investigated through measurements of species release. For example, quantitative measurements of the release of potassium from different types of burning biomass can be achieved using LIPF imaging technique or laser-induced breakdown spectroscopy. The effect of potassium on the heterogeneous reactions in the biomass fuels can be studied through motoring the release of key species, such as PAH, HCN and NH_3.

Finally, as a summary of the outlook, I would like to quote the title of a publication by Hupa et al. [3]:"*Biomass combustion technology development - It is all about chemical details.*".

Acknowledgement

Still, it is quite hard to believe that this will be the end of my four years' PhD study in Lund. Studying and living in this "small & peaceful village", Lund, will be one of the best memories in my life.

First of all, I would like to thank my main supervisor, Prof. Zhongshan Li, who gives me this chance to carry out PhD studies at Combustion Physics. You are an excellent supervisor who can always stimulate my research interest. I appreciate the countless hours in the past years, having the discussions on my PhD project and even the research work in the future, which is the most precious part for a young researcher. We exchanged lots of knowledge and opinions, not only about the academic research, but also about life, culture, history, and sometimes just the Swedish weather. I also want to give many thanks to my co-supervisors, Prof. Marcus Aldén and Dr. Christian Brackmann, who gave me a lot of support in my research activities.

I would like to thank Prof. Peter Glarborg and Prof. Hao Wu from Technical University of Denmark, and Prof. Mário Costa from Universidade de Lisboa. Without your help and advices, it would be impossible for me to complete this thesis work. I also want to express my gratitude to Prof. Zhihua Wang, Prof. Yong He, Dr. Kaidi Wan and Dr. Yingzhu Liu from Zhejiang University. The research team there always feels like home to me.

Thank you all the people that I have worked together with, especially those co-authors, Dr. Jesper Borggren, Dr. Tomas Leffler, Dina Hot, Dr. Rasmus Lyngbye Pedersen, Dr. Jim Larsson, Yuhe Zhang, Shen Li, Henrik Feuk, Dr. Qiang Gao, Dr. Shuang Chen, Dr. Hesameddin Fatehi, Ali Hosseinnia and Dr. Teresa Berdugo Vilches.

I am very glad that I could share the office with Dr. Rasmus Lyngbye Pedersen in the past four years. Hope you do still think I am a good officemate, even though I occupied the best position of the office during our whole PhD journey. I would like to thank all the friends in our division. At the beginning of my PhD studies, I received a lot of help from those senior students, Dr. Bo Zhou, Dr. Jiajian Zhu, Dina Hot and Dr. Jesper Borggren. I appreciate that we have the tradition of sharing experimental equipment in our division. The people who are willing to share their equipment with me are always the loveliest people: Dr. Chengdong Kong, Pär Samuelsson, Dr. Jinlong Gao, Dina

Bibliography

1. Knudsen, J.N., P.A. Jensen, and K. Dam-Johansen, *Transformation and Release to the Gas Phase of Cl, K, and S during Combustion of Annual Biomass.* Energy & Fuels, 2004. **18**(5): p. 1385-1399.

2. van Lith, S.C., et al., *Release to the Gas Phase of Inorganic Elements during Wood Combustion. Part 2: Influence of Fuel Composition.* Energy and Fuels, 2008. **22**(3): p. 1598-1609.

3. Hupa, M., O. Karlström, and E. Vainio, *Biomass combustion technology development – It is all about chemical details.* Proceedings of the Combustion Institute, 2017. **36**(1): p. 113-134.

4. Kassman, H., L. Bäfver, and L.-E. Åmand, *The importance of SO₂ and SO₃ for sulphation of gaseous KCl – An experimental investigation in a biomass fired CFB boiler.* Combustion and Flame, 2010. **157**(9): p. 1649-1657.

5. Kassman, H., F. Normann, and L.-E. Åmand, *The effect of oxygen and volatile combustibles on the sulphation of gaseous KCl.* Combustion and Flame, 2013. **160**(10): p. 2231-2241.

6. Kassman, H., et al., *Two strategies to reduce gaseous KCl and chlorine in deposits during biomass combustion — injection of ammonium sulphate and co-combustion with peat.* Fuel Processing Technology, 2013. **105**: p. 170-180.

7. Glarborg, P., *Hidden interactions—Trace species governing combustion and emissions.* Proceedings of the Combustion Institute, 2007. **31**(1): p. 77-98.

8. Thunman, H., et al., *Advanced biofuel production via gasification – lessons learned from 200 man-years of research activity with Chalmers' research gasifier and the GoBiGas demonstration plant.* Energy Science and Engineering, 2018. **6**(1): p. 6-34.

9. Glarborg, P. and P. Marshall, *Mechanism and modeling of the formation of gaseous alkali sulfates.* Combustion and Flame, 2005. **141**(1): p. 22-39.

10. Hindiyarti, L., et al., *An exploratory study of alkali sulfate aerosol formation during biomass combustion.* Fuel, 2008. **87**(8): p. 1591-1600.

11. Li, B., et al., *Post-flame gas-phase sulfation of potassium chloride.* Combustion and Flame, 2013. **160**(5): p. 959-969.

12. Ekvall, T., et al., *K–Cl–S chemistry in air and oxy-combustion atmospheres.* Proceedings of the Combustion Institute, 2017. **36**(3): p. 4011-4018.

13. Rosser, W.A., S.H. Inami, and H. Wise, *The effect of metal salts on premixed hydrocarbon—air flames.* Combustion and Flame, 1963. **7**: p. 107-119.
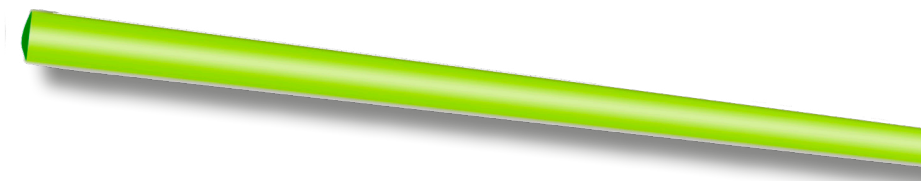
14. Slack, M., et al., *Potassium kinetics in heavily seeded atmospheric pressure laminar methane flames.* Combustion and Flame, 1989. **77**(3): p. 311-320.

15. Leffler, T., et al., *Experimental investigations of potassium chemistry in premixed flames.* Fuel, 2017. **203**: p. 802-810.

16. Reaction Design, *CHEMKIN-PRO 15131* 2013: San Diego.

17. Smith, G.P., et al. *GRI-Mech 3.0.* Available from: http://www.me.berkeley.edu/gri_mech/.

18. Garba, M.U., et al., *Prediction of potassium chloride sulfation and its effect on deposition in biomass-fired boilers.* Energy & Fuels, 2012. **26**(11): p. 6501-6508.

19. Prucker, S., W. Meier, and W. Stricker, *A flat flame burner as calibration source for combustion research: Temperatures and species concentrations of premixed H$_2$/air flames.* Review of Scientific Instruments, 1994. **65**(9): p. 2908-2911.

20. Snelleman, W. and J.A. Smit, *A Flame as a Secondary Standard of Temperature.* Metrologia, 1968. **4**(3): p. 123.

21. Hsu, L.-J., et al., *Sodium and Potassium Released from Burning Particles of Brown Coal and Pine Wood in a Laminar Premixed Methane Flame Using Quantitative Laser-Induced Breakdown Spectroscopy.* Applied Spectroscopy, 2011. **65**(6): p. 684-691.

22. Borggren, J., et al., *Diode laser-based thermometry using two-line atomic fluorescence of indium and gallium.* Applied Physics B, 2017. **123**(12): p. 278.

23. Whiddon, R., et al., *Vapor phase tri-methyl-indium seeding system suitable for high temperature spectroscopy and thermometry.* Review of Scientific Instruments, 2015. **86**(9): p. 093107.

24. Weng, W., et al., *Quantitative Measurement of Atomic Potassium in Plumes over Burning Solid Fuels Using Infrared-Diode Laser Spectroscopy.* Energy & Fuels, 2017. **31**(3): p. 2831-2837.

25. Qu, Z., et al., *Tunable Diode Laser Atomic Absorption Spectroscopy for Detection of Potassium under Optically Thick Conditions.* Analytical Chemistry, 2016. **88**(7): p. 3754-3760.

26. Schlosser, E., et al., *In situ detection of potassium atoms in high-temperature coal-combustion systems using near-infrared-diode lasers.* Spectrochimica Acta Part A: Molecular and Biomolecular Spectroscopy, 2002. **58**(11): p. 2347-2359.

27. Sansonetti, J.E., *Wavelengths, Transition Probabilities, and Energy Levels for the Spectra of Potassium (KI through KXIX).* Journal of Physical and Chemical Reference Data, 2008. **37**(1): p. 7-96.

28. Leffler, T., et al., *Development of an alkali chloride vapour-generating apparatus for calibration of ultraviolet absorption measurements.* Review of Scientific Instruments, 2017. **88**(2): p. 023112.

29. Davidovits, P. and D.C. Brodhead, *Ultraviolet Absorption Cross Sections for the Alkali Halide Vapors.* Journal of Chemical Physics, 1967. **46**(8): p. 2968-2973.

30. Weng, W., et al., *Spectrally Resolved UV Absorption Cross-Sections of Alkali Hydroxides and Chlorides Measured in Hot Flue Gases.* Applied Spectroscopy, 2018: p. 0003702818763819.

31. Vandaele, A.C., C. Hermans, and S. Fally, *Fourier transform measurements of SO_2 absorption cross sections: II.: Temperature dependence in the 29000–44000cm−1 (227–345nm) region.* Journal of Quantitative Spectroscopy and Radiative Transfer, 2009. **110**(18): p. 2115-2126.

32. Vattulainen, J., et al., *Experimental Determination of SO_2, C_2H_2, and O_2 UV Absorption Cross Sections at Elevated Temperatures and Pressures.* Applied Spectroscopy, 1997. **51**(9): p. 1311-1315.

33. Grosch, H., et al., *Hot gas flow cell for optical measurements on reactive gases.* Journal of Quantitative Spectroscopy and Radiative Transfer, 2013. **130**: p. 392-399.

34. Mellqvist, J. and A. Rosén, *DOAS for flue gas monitoring—I. Temperature effects in the U.V./visible absorption spectra of NO, NO_2, SO_2 and NH_3.* Journal of Quantitative Spectroscopy and Radiative Transfer, 1996. **56**(2): p. 187-208.

35. Gao, Q., et al., *Gas Temperature Measurement Using Differential Optical Absorption Spectroscopy (DOAS).* Applied Spectroscopy, 2018. **72**(7): p. 1014-1020.

36. Leffler, T., et al., *Laser-Induced Photofragmentation Fluorescence Imaging of Alkali Compounds in Flames.* Applied Spectroscopy, 2017. **71**(6): p. 1289-1299.

37. Oldenborg, R.C. and S.L. Baughcum, *Photofragment fluorescence as an analytical technique: application to gas-phase alkali chlorides.* Analytical Chemistry, 1986. **58**(7): p. 1430-1436.

38. Sorvajärvi, T., et al., *In Situ Measurement Technique for Simultaneous Detection of K, KCl, and KOH Vapors Released during Combustion of Solid Biomass Fuel in a Single Particle Reactor.* Applied Spectroscopy, 2014. **68**(2): p. 179-184.

39. Gao, J., *Diagnostics on combustion and plasma for optimized thermochemical applications*, in *Department of physics*. 2018, Lund University.

40. *LIEBASE, version 2.1.* 2013 2013; Available from: https://www.sri.com/contact /form/lifbase.

41. Thunman, H., et al., *Advanced biofuel production via gasification – lessons learned from 200 man-years of research activity with Chalmers' research gasifier and the GoBiGas demonstration plant.* Energy Science & Engineering, 2018. **6**(1): p. 6-34.

42. Ciajolo, A., A. D'Anna, and R. Barbella, *PAH and High Molecular Weight Species Formed in a Premixed Methane Flame.* Combustion Science and Technology, 1994. **100**(1-6): p. 271-281.

LUND
UNIVERSITY